

Thermoelectric fluctuations of interfering Majorana bound states

Sergey Smirnov

*P. N. Lebedev Physical Institute of the Russian Academy of Sciences, 119991 Moscow, Russia**

(Dated: March 7, 2025)

Nonequilibrium states produced by electric and thermal voltages (V , V_T) provide a straightforward insight into underlying degrees of freedom of composite nanostructures and are of particular interest to probe Majorana bound states. Here we explore fluctuations of thermoelectric currents at finite frequencies ω in a quantum dot coupled to two interfering Majorana bound states. At small V we find that in the emission spectra the differential thermoelectric quantum noise $\partial S^>/\partial V_T$ shows an antiresonance whereas in the absorption spectra Majorana interference induces an antiresonance-resonance pair. At large V this pair is preserved whereas the emission antiresonance turns into an antiresonance-resonance pair identical to the absorption one making $\partial S^>/\partial V_T$ antisymmetric in the frequency ω . This antisymmetry distinguishes Majorana behavior from the one induced by Andreev bound states and does not break at higher temperatures making it attractive for experiments on Majorana interference via thermoelectric fluctuation response.

I. INTRODUCTION

Probing Majorana bound states (MBSs) in diverse systems [1–12] via various advanced techniques enriches our knowledge about many remarkable aspects of Majorana nanosystems and creates a significant potential for future experimental implementations. Involving a complex interplay between various degrees of freedom such nanosystems, on one side, are appealing for quantum computations [13], based on the unique non-Abelian exchange statistics of MBSs (as opposed to the Abelian one of the Majorana fermions [14, 15] in the particle physics), and, on the other side, they exhibit exceptional physical properties which may be accessed by proper measurements. The latter side of exploring Majorana nanosystems offers a great freedom to explore MBSs via numerous and essentially independent physical observables which may be predicted in theory and would be relevant for state-of-the-art experiments.

For example, equilibrium states of nanoscopic devices involving MBSs may be addressed via their linear conductance or entropy which provide quantum transport or thermodynamic probes, respectively. These probes are fundamentally distinct. The most essential difference between them, among others, manifests in whether the corresponding outcomes admit unambiguous conclusions. Whereas the fractional Majorana entropy [16–19] cannot be ascribed to non-Majorana quasiparticles, the values of various linear conductances, predicted for systems with MBSs, may also be obtained in experiments where MBSs are absent [20, 21]. Nevertheless, the advantage of the quantum transport approach consists in its technological flexibility which allows one to straightforwardly apply it to various systems with MBSs [22–24]. Quantum thermodynamic measurements of the entropy in nanoscopic

systems with MBSs are currently an experimental challenge whose solution appears quite plausible as one may assume on the basis of the notable progress [25–31] in theoretical and experimental research devoted to the entropy of nanoscopic systems whose degrees of freedom do not yet involve MBSs.

Due to its experimental appeal quantum transport is of special interest and is often used to analyze MBSs not only via linear conductances but also via differential conductances, or in general, via mean electric currents beyond the linear response approach [32–63]. When Majorana nanosystems are coupled to contacts with different temperatures, one gets an opportunity to study thermoelectric mean currents [64–80] providing information independent of pure electric behavior of MBSs. In fact, strongly nonequilibrium Majorana systems beyond the linear response regime provide a wider spectrum of measurements which are not restricted only by mean currents. When the fluctuation-dissipation theorem is not applicable, as is the case in strong nonequilibrium, electric and thermoelectric fluctuations bring information unavailable in conductance measurements and proper current-current correlation functions allow one to analyze MBSs from a qualitatively different side. Indeed, one may additionally investigate MBSs via the electric [81–94] and thermoelectric [95–97] shot and quantum noise which are physical observables of experimental relevance. Shot noise experiments have already started dealing with Majorana nanosystems [98]. Experimental measurements of the differential quantum noise at finite frequencies have been previously performed [99] to study the Kondo effect in a quantum dot (QD) and one may naturally assume that the techniques used for these measurements could be adapted to QDs coupled to MBSs. It is important to note that this coupling often involves Majorana tunneling phases which, on one side, are important degrees of freedom to drive Majorana qubits [100, 101] and, on the other side, are responsible for various interference effects resulting in a remarkable behavior of the shot and quantum noise [91, 94].

Various important physical observables characterizing

* 1) sergej.physik@gmail.com

2) sergey.smirnov@physik.uni-regensburg.de

3) ssmirnov@sci.lebedev.ru

random deviations of currents from their mean values, such as the static shot noise or finite frequency quantum noise, exhibit a rather nontrivial behavior in nonequilibrium states produced by both bias and thermal voltages [95–97]. In particular, in the absence of Majorana interference effects, the static (zero-frequency) differential thermoelectric shot noise has been investigated in Ref. [95], the differential thermoelectric quantum noise at finite frequencies has been presented in Ref. [96] and the zero-frequency differential shot noise, more specifically its crossover behavior, as a function of the thermal voltage has been explored in Ref. [97]. In the presence of Majorana interference effects but in the absence of thermal voltages, that is pure electric behavior of the zero-frequency differential shot noise and finite frequency differential quantum noise, has been analyzed in, respectively, Refs. [91] and [94]. More interesting phenomena are expected when Majorana interference effects emerge in nanoscopic systems driven by both electric and thermal voltages. When the competition between electrically and thermally excited quasiparticle flows is additionally boosted by Majorana interference effects, nonequilibrium states resulting from this complex interplay acquire an intricate nature. As such, they represent an original source of information about a unique fluctuation response of interfering MBSs, particularly, at finite frequencies. These fluctuations may be probed via quantum transport techniques measuring, for example, such a physical observable as the finite frequency quantum noise which, to our knowledge, has never been addressed for interfering MBSs in thermoelectric nonequilibrium.

In this work we consider a QD coupled to two MBSs and explore the behavior of the differential thermoelectric quantum noise $\partial S^>(\omega, V, V_T, \Delta\phi)/\partial V_T$ defined as the derivative of the greater noise correlation function with respect to the thermal voltage V_T . The analysis is performed numerically at finite frequencies ω for both the emission ($\omega < 0$) and absorption ($\omega > 0$) parts of the spectra and focuses particularly on the behavior of the interfering MBSs, that is on the one arising for finite values of the Majorana tunneling phase difference $\Delta\phi$. In the regime of small bias voltages V it is shown that for well separated energy scales there develops an antiresonance in the emission part of the spectra and that it is located around $\hbar\omega = -|eV|/2$. This emission antiresonance results from the Majorana interference because it is strongly suppressed for $\Delta\phi = 0$. In the absorption part of the spectra there develops a pair antiresonance-resonance located around $\hbar\omega = |eV|/2$. Like the emission antiresonance, this pair is of pure Majorana interference nature since it is also strongly suppressed for $\Delta\phi = 0$. Thus in the regime of small bias voltages and for $\Delta\phi \neq 0$ the emission and absorption spectra are not related to each other. This is in contrast to the case where a QD is effectively coupled to a single MBS and the emission and absorption spectra turn out to be symmetrically related in the regime of small bias voltages [96]. Further, it is found that the absorption antiresonance-resonance pair located

at $\hbar\omega = |eV|/2$ survives in the regime of large bias voltages but with the exactly twice reduced amplitudes of the antiresonance and resonance. At the same time the emission antiresonance is fully destroyed by large bias voltages and transforms into an emission antiresonance-resonance pair located at $\hbar\omega = -|eV|/2$. This emission antiresonance-resonance pair is fully identical to the absorption one for any finite value of $\Delta\phi$. This transformation of the emission spectra at large bias voltages is of particular importance. Indeed, since the differential thermoelectric quantum noise is strongly suppressed outside vicinities of the frequencies $\hbar\omega = \pm|eV|/2$, we find that $\partial S^>(-\omega, V, V_T, \Delta\phi)/\partial V_T = -\partial S^>(\omega, V, V_T, \Delta\phi)/\partial V_T$, that is the absorption and emission spectra are antisymmetrically related in the regime of large bias voltages for any finite value of $\Delta\phi$. Finally, we investigate the regime of high bias voltages and temperatures which might be of experimental relevance. Here, our estimate shows that the temperature may be around 60 mK (see the details at the end of Section V with the notations and parameter regime defined in the main text) which is well within the temperature range used for quantum transport experiments. It is shown that the antisymmetric relation between the absorption and emission spectra is also observed in this regime in the presence of the Majorana interference ($\Delta\phi \neq 0$). In contrast, we demonstrate that Andreev bound states (ABSs) break this relation, $\partial S^>(-\omega, V, V_T, \Delta\phi)/\partial V_T \neq -\partial S^>(\omega, V, V_T, \Delta\phi)/\partial V_T$, and their thermoelectric fluctuation response at finite frequencies ω is qualitatively different from the one of interfering MBSs.

The paper is organized as follows. In Section II we specify the system via its Hamiltonian involving tunneling between a QD and two MBSs which may interfere. Thermoelectric nonequilibrium induced by coupling of the QD to contacts with different chemical potentials and temperatures is also specified here. To describe these nonequilibrium states we apply the Keldysh technique in Section III. The results obtained for the differential thermoelectric quantum noise are presented in Section IV in various regimes including low bias voltages, large bias voltages and also large temperatures in the presence of the Majorana interference. Finally, we conclude the paper in Section V where we also estimate the values of the temperature at which experiments could be performed to reveal Majorana interference patterns in the differential thermoelectric quantum noise at finite frequencies.

II. HAMILTONIAN OF THE SYSTEM WITH INTERFERING MAJORANA BOUND STATES

Let us start with the full Hamiltonian of a system whose behavior is essentially determined by Majorana interference effects:

$$\hat{H} = \hat{H}_{\text{QD}} + \hat{H}_{\text{C}} + \hat{H}_{\text{TS}} + \hat{H}_{\text{QD-C}} + \hat{H}_{\text{QD-TS}}. \quad (1)$$

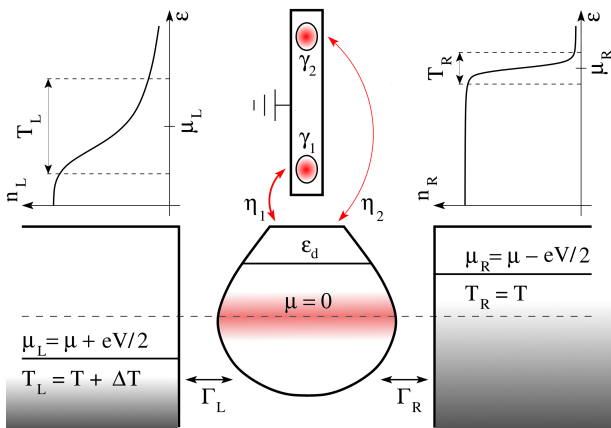


FIG. 1. An illustration of the physical system modeled by the full Hamiltonian in Eq. (1). The QD with the energy level ϵ_d is coupled with the coupling strengths $\Gamma_{L,R}$ to, respectively, the left and right contacts characterized by the chemical potentials $\mu_{L,R}$ and temperatures $T_{L,R}$. The grounded TS supports two MBSs $\gamma_{1,2}$ coupled to the QD. This coupling is characterized by the tunneling matrix elements $\eta_{1,2}$ with the amplitudes $|\eta_1| \gg |\eta_2|$ modeling an asymmetric location of the Majorana modes with respect to the QD (see, for example, Ref. [102]).

The system consists of a QD, metallic contacts, and a topological superconductor (TS) which are modeled by the Hamiltonians \hat{H}_{QD} , \hat{H}_C and \hat{H}_{TS} , respectively.

The Hamiltonian of the isolated QD,

$$\hat{H}_{\text{QD}} = \epsilon_d d^\dagger d, \quad (2)$$

represents an electronic system with one non-degenerate single-particle energy level. Its energy ϵ_d relative to the equilibrium chemical potential μ may be tuned via a proper gate voltage. The fermionic operators corresponding to the single-particle state of the QD, d and d^\dagger , obey the conventional anticommutation relations,

$$\{d, d\} = 0, \quad \{d, d^\dagger\} = 1. \quad (3)$$

As described below, the QD is coupled via tunneling to a closely located TS (see, *e.g.*, Ref. [102] for a technological implementation). The topological phase with two MBSs at the ends of the TS emerges in a strong magnetic field which also makes the energy spectrum of the QD non-degenerate. Indeed, computations [103] based on the numerical renormalization group indicate that in a strong magnetic field the QD behaves as the one where the spin degeneracy is removed and the Kondo effect is fully absent. Thus the Majorana physics is properly captured by the non-degenerate QD model in Eq. (2) when it is combined with a suitable model of the TS coupled to the QD (see also Ref. [104]).

The Hamiltonian of the two, left (L) and right (R), isolated metallic contacts,

$$\hat{H}_C = \sum_{l=\{L,R\}} \sum_k \epsilon_k c_{lk}^\dagger c_{lk}, \quad (4)$$

describes non-interacting fermionic systems. The operators corresponding to the states of these systems also obey the conventional anticommutation relations,

$$\{c_{lk}, c_{l'k'}\} = 0, \quad \{c_{lk}, c_{l'k'}^\dagger\} = \delta_{ll'} \delta_{kk'}. \quad (5)$$

The contacts are assumed to be massive so that their energy spectra, $\epsilon_{L,k} = \epsilon_{R,k} = \epsilon_k$, are continuous. They are characterized by the corresponding density of states $\nu(\epsilon)$ which is, in fact, sufficient to calculate various physical observables. We neglect the energy dependence of the contacts density of states,

$$\nu(\epsilon) \approx \frac{1}{2} \nu_C. \quad (6)$$

This assumption is often justified since in many quantum transport experiments measurements are performed in the energy range where the density of states in the metallic contacts does not vary too much to produce qualitative observable effects.

Both metallic contacts are in equilibrium states. These states are specified by the Fermi-Dirac distributions:

$$n_{L,R}(\epsilon) = \frac{1}{\exp\left(\frac{\epsilon - \mu_{L,R}}{k_B T_{L,R}}\right) + 1}, \quad (7)$$

where $\mu_{L,R}$ is the chemical potential and $T_{L,R}$ the temperature of the left or right metallic contact, respectively. In general the equilibrium states of the left and right contacts are different, that is $\mu_L \neq \mu_R$ and $T_L \neq T_R$. The difference between the chemical potentials is specified via the bias voltage V applied to the two contacts:

$$\mu_{L,R} = \mu \pm eV/2, \quad (8)$$

where we have used $eV < 0$ to obtain the numerical results discussed in Sec. IV. The temperatures are chosen to specify the left contact as hot and the right one as cold,

$$T_L = T + \Delta T, \quad T_R = T, \quad \Delta T \geq 0. \quad (9)$$

To obtain the numerical results presented in Sec. IV we have parameterized the temperature difference ΔT by a thermal voltage V_T between the contacts:

$$eV_T \equiv k_B \Delta T. \quad (10)$$

The low-energy Hamiltonian of the isolated TS,

$$\hat{H}_{\text{TS}} = \frac{i}{2} \xi \gamma_2 \gamma_1, \quad (11)$$

assumes that in its topological phase there arise two MBSs located at its ends. Here the self-adjoint fermionic operators,

$$\gamma_{1,2}^\dagger = \gamma_{1,2}, \quad (12)$$

corresponding to the low-energy states of the TS obey the Majorana, or Clifford algebra [105], anticommutation relations,

$$\{\gamma_j, \gamma_{j'}\} = 2\delta_{jj'}, \quad j, j' = 1, 2. \quad (13)$$

A finite value of the energy ξ in Eq. (11) corresponds to a finite overlap between the MBSs. The TS is assumed to be grounded.

The QD interacts with the metallic contacts and TS via tunneling mechanisms modeled by the tunneling Hamiltonians $\hat{H}_{\text{QD-C}}$ and $\hat{H}_{\text{QD-TS}}$, respectively.

The Hamiltonian for the tunneling between the QD and metallic contacts,

$$\hat{H}_{\text{QD-C}} = \sum_{l=\{L,R\}} \mathcal{T}_l \sum_k c_{lk}^\dagger d + \text{H.c.}, \quad (14)$$

uses the approximation

$$\mathcal{T}_{lk} \approx \mathcal{T}_l \quad (15)$$

for the tunneling matrix elements whose dependence on k is sufficiently weak in the energy range relevant for quantum transport measurements. The tunneling interaction between the QD and metallic contacts appears via the energy scales

$$\Gamma_{L,R} = \pi\nu_C |\mathcal{T}_{L,R}|^2. \quad (16)$$

The sum of these energies,

$$\Gamma = \Gamma_L + \Gamma_R, \quad (17)$$

determines the escape rate of quasiparticles from the QD into the metallic contacts. To simplify the model, in our numerical calculations we have assumed that the QD is coupled symmetrically to the left and right contacts,

$$\Gamma_L = \Gamma_R. \quad (18)$$

The Hamiltonian for the tunneling between the QD and TS,

$$\hat{H}_{\text{QD-TS}} = \eta_1^* d^\dagger \gamma_1 + \eta_2^* d^\dagger \gamma_2 + \text{H.c.}, \quad (19)$$

includes in general two interactions, namely, between the QD and the two Majorana modes, γ_1 and γ_2 . The Majorana tunneling matrix elements,

$$\eta_{1,2} = |\eta_{1,2}| e^{i\phi_{1,2}}, \quad (20)$$

play the central role in the present research because they are responsible for various interference effects in nanostructures with $|\eta_1| \neq 0$ and $|\eta_2| \neq 0$. The Majorana interference arises when the tunneling phases become unequal,

$$\Delta\phi \equiv \phi_1 - \phi_2 \neq 0. \quad (21)$$

For more clarity the above mathematical description of the system is represented graphically in Fig. 1. To be specific, in our numerical calculations we assume a nanostructure similar to the one in Ref. [102] where the QD is located asymmetrically with respect to the two MBSs, *i.e.* much closer to one Majorana mode than to the other.

The numerical results presented in Sec. IV have been obtained for $|\eta_1| \gg |\eta_2|$ that is the Majorana mode γ_1 has been chosen as the closest to the QD. We note, that even a very weak coupling between γ_2 and the QD becomes crucial for fluctuations of thermoelectric currents induced by both V and V_T . Indeed, even when $|\eta_2|$ is several orders of magnitude smaller than $|\eta_1|$, the thermoelectric quantum noise at finite frequencies acquires a very strong dependence on the Majorana tunneling phase difference $\Delta\phi$ as demonstrated by the numerical results presented in Sec. IV.

III. KELDYSH FORMALISM FOR QUANTUM FLUCTUATIONS OF NONEQUILIBRIUM THERMOELECTRIC CURRENTS

If the chemical potentials and temperatures of the metallic contacts do not vary in time, the nanoscopic system specified in Sec. II will be brought into a stationary nonequilibrium state produced by both the bias and thermal voltages. To deal with stationary nonequilibrium we apply the formalism of the Keldysh field integral [106] which is a flexible mathematical tool developed on the basis of the original Keldysh technique [107]. In particular, it allows one to consistently generate current-current correlation functions which we need in this work to analyze the thermoelectric quantum noise at finite frequencies in the presence of Majorana interference effects. Although the Keldysh field integral is well described in various textbooks [106], below we briefly remind some of its steps in the context of our problem.

Due to the fermionic nature of our system the Keldysh field integral is performed over the Grassmann fields and their conjugate partners, $(\psi, \bar{\psi})$, $(\phi_{lk}, \bar{\phi}_{lk})$ and $(\zeta, \bar{\zeta})$, appearing after the standard mapping [106] from the operators (d, d^\dagger) , (c_{lk}, c_{lk}^\dagger) and (γ_1, γ_2) to their eigenvalues representing the states of the QD, contacts and TS, respectively. Here and below the Grassmann conjugation (G.c.) is denoted with an upper bar. The closed time contour may be parameterized by the real time t and the branch index q labeling its forward ($q = +$) and backward ($q = -$) branches. Then the Keldysh generating functional is written as a field integral,

$$\mathcal{Z}[\mathcal{J}_{lq}(t)] = \int \mathcal{D}[\bar{\Phi}_q(t), \Phi_q(t)] e^{\frac{i}{\hbar} S_K[\mathcal{J}_{lq}(t)]}, \quad (22)$$

over the corresponding Grassmann fields and their conjugate partners,

$$\{\Phi_q(t); \bar{\Phi}_q(t)\} \equiv \{\psi_q(t), \phi_{lkq}(t), \zeta_q(t); \bar{\psi}_q(t), \bar{\phi}_{lkq}(t), \bar{\zeta}_q(t)\}, \quad (23)$$

defined on the real time axis t . The Keldysh action S_K ,

$$\begin{aligned} S_K[\mathcal{J}_{lq}(t)] = & S_{\text{QD}}[\bar{\psi}_q(t), \psi_q(t)] + \\ & + S_{\text{C}}[\bar{\phi}_{lkq}(t), \phi_{lkq}(t)] + S_{\text{TS}}[\bar{\zeta}_q(t), \zeta_q(t)] + \\ & + S_{\text{QD-C}}[\bar{\psi}_q(t), \bar{\phi}_{lkq}(t); \psi_q(t), \phi_{lkq}(t)] + \\ & + S_{\text{QD-TS}}[\bar{\psi}_q(t), \bar{\zeta}_q(t); \psi_q(t), \zeta_q(t)] + S_{\text{SRC}}[\mathcal{J}_{lq}(t)], \end{aligned} \quad (24)$$

is a functional of the source field $\mathcal{J}_{lq}(t)$ introduced via the source action S_{SRC} to generate current-current correlators. Note, that the generating functional is properly normalized,

$$\mathcal{Z}[\mathcal{J}_{lq}(t) = 0] = 1. \quad (25)$$

After the Keldysh rotation [106] the Grassmann fields on the forward and backward branches are combined into the retarded and advanced components. This transformation brings the actions of the QD, contacts and TS, denoted as S_{QD} , S_{C} and S_{TS} , into the conventional 2×2 matrix form [106]. The action describing tunneling processes between the QD and contacts mixes the Grassmann fields $\{\bar{\psi}_q(t), \psi_q(t)\}$ and $\{\bar{\phi}_{lkq}(t), \phi_{lkq}(t)\}$:

$$\begin{aligned} & S_{\text{QD-C}}[\bar{\psi}_q(t), \bar{\phi}_{lkq}(t); \psi_q(t), \phi_{lkq}(t)] = \\ & = - \int_{-\infty}^{\infty} dt \sum_{l=\{L,R\}} \sum_{k,q} [\mathcal{T}_{lq} \bar{\phi}_{lkq}(t) \psi_q(t) + \text{G.c.}]. \end{aligned} \quad (26)$$

The action taking into account the tunneling interaction between the QD and TS mixes the Grassmann fields $\{\bar{\psi}_q(t), \psi_q(t)\}$ with $\{\bar{\zeta}_q(t), \zeta_q(t)\}$,

$$\begin{aligned} & S_{\text{QD-TS}}[\bar{\psi}_q(t), \bar{\zeta}_q(t); \psi_q(t), \zeta_q(t)] = \\ & = - \int_{-\infty}^{\infty} dt \sum_q q \{ \eta_1^* [\bar{\psi}_q(t) \zeta_q(t) + \bar{\psi}_q(t) \bar{\zeta}_q(t)] + \\ & + i\eta_2^* [\bar{\psi}_q(t) \zeta_q(t) + \bar{\psi}_{-q}(t) \bar{\zeta}_{-q}(t)] + \text{G.c.} \}, \end{aligned} \quad (27)$$

and involves the Majorana tunneling phases ϕ_1 and ϕ_2 through the matrix elements η_1 and η_2 . This tunneling action is of particular importance because various Majorana interference effects in physical observables result eventually from Eq. (27).

As mentioned above, the second quantized operators of the QD, contacts and TS map to the corresponding Grassmann-valued fields. As a result, the operators of physical observables map to the corresponding functions of these fields. In particular, the current operator in contact $l = \{L, R\}$,

$$\hat{I}_l = \frac{ie}{\hbar} \sum_k (\mathcal{T}_{lk} c_k^\dagger d - \text{H.c.}), \quad (28)$$

maps to the Grassmann-valued field

$$I_{lq}(t) = \frac{ie}{\hbar} \sum_k [\mathcal{T}_{lk} \bar{\phi}_{lkq}(t) \psi_q(t) - \text{G.c.}]. \quad (29)$$

Using this field one may define the source action S_{SRC} ,

$$S_{\text{SRC}}[\mathcal{J}_{lq}(t)] = - \int_{-\infty}^{\infty} dt \sum_{l=\{L,R\}} \sum_q \mathcal{J}_{lq}(t) I_{lq}(t), \quad (30)$$

to generate current-current correlators,

$$\langle I_{lq}(t) I_{l'q'}(t') \rangle_0 = (i\hbar)^2 \frac{\delta^2 \mathcal{Z}[\mathcal{J}_{lq}(t)]}{\delta \mathcal{J}_{lq}(t) \delta \mathcal{J}_{l'q'}(t')} \Big|_{\mathcal{J}_{lq}(t)=0}, \quad (31)$$

where the averaging $\langle \dots \rangle_0$ is defined with respect to the Keldysh action

$$S_{\text{K}}^{(0)} \equiv S_{\text{K}}[\mathcal{J}_{lq}(t) = 0], \quad (32)$$

that is

$$\begin{aligned} & \langle I_{l_1 q_1}(t_1) \cdots I_{l_n q_n}(t_n) \rangle_0 \equiv \\ & \equiv \int \mathcal{D}[\bar{\Phi}_q(t), \Phi_q(t)] e^{\frac{i}{\hbar} S_{\text{K}}^{(0)}} I_{l_1 q_1}(t_1) \cdots I_{l_n q_n}(t_n). \end{aligned} \quad (33)$$

Note, that in stationary nonequilibrium the average in Eq. (33) depends on the temporal arguments only through the differences $t_1 - t_k$, $k = 2, \dots, n$. To obtain the mean current in contact $l = \{L, R\}$ one may choose any branch q in Eq. (29) since after averaging the dependence on q disappears,

$$I_l(V, V_T, \Delta\phi) = \langle I_{lq}(t) \rangle_0 = i\hbar \frac{\delta \mathcal{Z}[\mathcal{J}_{lq}(t)]}{\delta \mathcal{J}_{lq}(t)} \Big|_{\mathcal{J}_{lq}(t)=0}. \quad (34)$$

In general one may consider various current-current correlators either within a given contact or between different contacts. To be specific, in what follows we will investigate fluctuations of the thermoelectric current in the left metallic contact and characterize these fluctuations by the quantum noise specified via the greater current-current correlator:

$$S^>(t - t', V, V_T, \Delta\phi) \equiv \langle \delta I_{L-}(t) \delta I_{L+}(t') \rangle_0, \quad (35)$$

where

$$\delta I_{Lq}(t) \equiv I_{Lq}(t) - I_L(V, V_T, \Delta\phi) \quad (36)$$

is the Grassmann-valued field corresponding to the current deviations from the mean value. The calculation of the average $\langle \dots \rangle_0$ in Eq. (35) is performed using conventional Wick's theorem as in Ref. [95] where one can find more technical details.

In the frequency domain,

$$S^>(\omega, V, V_T, \Delta\phi) = \int_{-\infty}^{\infty} dt e^{i\omega t} S^>(t, V, V_T, \Delta\phi), \quad (37)$$

the quantum noise provides a unique way to explore Majorana interference effects via a thermoelectric fluctuation response at finite frequencies in both the absorption,

$$S^{\text{ab}}(\omega, V, V_T, \Delta\phi) = S^>(\omega > 0, V, V_T, \Delta\phi), \quad (38)$$

and emission,

$$S^{\text{em}}(\omega, V, V_T, \Delta\phi) = S^>(\omega < 0, V, V_T, \Delta\phi), \quad (39)$$

photon spectra. To be specific, below we address the fluctuation response encoded at finite frequencies in the differential thermoelectric quantum noise defined as the derivative with respect to the thermal voltage, $\partial S^>(\omega, V, V_T, \Delta\phi) / \partial V_T$, which might be of experimental interest similarly to the differential quantum noise [99] defined as the derivative with respect to the bias voltage.

IV. FINITE FREQUENCY BEHAVIOR OF THE DIFFERENTIAL THERMOELECTRIC QUANTUM NOISE IN VARIOUS REGIMES

To obtain the results presented in this section we have implemented two numerical approaches. In the first approach we have analytically calculated all the necessary derivatives over the thermal voltage V_T since it enters only through the Fermi-Dirac distribution of the left metallic contact as may be seen in Eqs. (7), (9) and (10). After that numerical integrations have been used to obtain $\partial S^>(\omega, V, V_T, \Delta\phi)/\partial V_T$. In the second approach, numerical integrations are first performed to obtain $S^>(\omega, V, V_T, \Delta\phi)$. After that we have used finite differences to numerically calculate the derivative $\partial S^>(\omega, V, V_T, \Delta\phi)/\partial V_T$. In different physical regimes the difference between the computational times of these two approaches may be significant and we have always used the faster one. It is important to note that various outputs obtained by the two approaches have been compared and found to be identical. This provides a good verification for the numerical results presented below.

To study the universal Majorana behavior, that is the one independent of ϵ_d , the numerical calculations have been restricted to the regime in which one of the Majorana tunneling amplitudes, $|\eta_1|$ or $|\eta_2|$, is the largest energy scale of the problem. Since in Sec. II we have assumed $|\eta_1| \gg |\eta_2|$, we have chosen $|\eta_1|$ as the largest energy scale:

$$|\eta_1| > \max\{|\epsilon_d|, k_B T, |\eta_2|, \xi, \Gamma, eV_T, |eV|\}. \quad (40)$$

In the universal Majorana regime specified by Eq. (40) physical observables do not depend on ϵ_d and thus its value may be chosen arbitrarily within this regime. The numerical results presented below have been obtained for the case $\epsilon_d > 0$ but they remain the same also for the case $\epsilon_d < 0$. In possible experiments, however, the magnetic field inducing the topological phase with emerging MBSs may strongly but still incompletely suppress the Kondo correlations in QDs with $\epsilon_d < 0$ and, as a result, the Kondo universality [108–110] may superimpose on the Majorana one. Thus, to avoid any possible interplay [111–114] between the Kondo effect and MBSs, experiments with $\epsilon_d > 0$ would be preferable to observe phenomena driven by exclusively MBSs.

In Fig. 2 we show the differential thermoelectric quantum noise as a function of the frequency in the domain $\omega < 0$ (emission noise) for small bias voltages, $|eV| \ll \Gamma$. Here, in addition to the resonance located at $\hbar\omega = -|eV|$, which has been discussed previously [96], there arises qualitatively new behavior around the frequency $\hbar\omega = -|eV|/2$. When the energy scales are well separated, that is when $k_B T$ is several orders of magnitude less than $|eV|$ (in the regime $eV_T \ll k_B T \ll |eV|$) or eV_T is several orders of magnitude less than $|eV|$ (in the regime $k_B T \ll eV_T \ll |eV|$), there develops an antiresonance with its minimum located at $\hbar\omega = -|eV|/2$. For small values of the Majorana tunneling phase difference

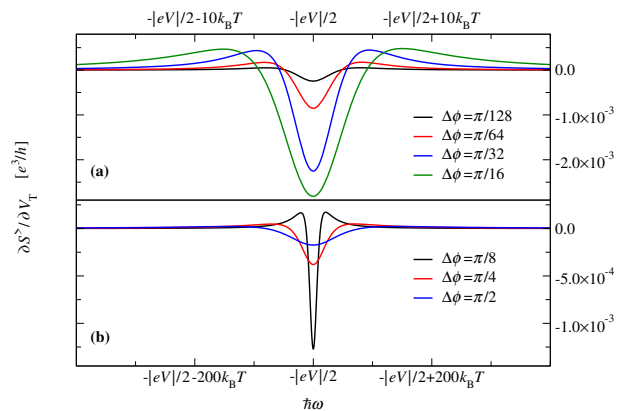


FIG. 2. Frequency dependence of the differential thermoelectric quantum noise, $\partial S^>(\omega, V, V_T, \Delta\phi)/\partial V_T$, in a vicinity of the frequency $\hbar\omega = -|eV|/2$ (emission noise, domain $\omega < 0$) for small bias voltages, $|eV| \ll \Gamma$, and for various values of the Majorana tunneling phase difference $\Delta\phi$. Specifically, for all the curves $|eV|/\Gamma = 10^{-2}$ and, in Panel (a), $\Delta\phi = \pi/128$ (black), $\Delta\phi = \pi/64$ (red), $\Delta\phi = \pi/32$ (blue), $\Delta\phi = \pi/16$ (green), in Panel (b), $\Delta\phi = \pi/8$ (black), $\Delta\phi = \pi/4$ (red), $\Delta\phi = \pi/2$ (blue). The values of the other parameters: $\epsilon_d/\Gamma = 10$, $k_B T/\Gamma = 10^{-7}$, $eV_T/\Gamma = 10^{-9}$, $|\eta_1|/\Gamma = 10^3$, $|\eta_2|/\Gamma = 10^{-3}$, $\xi/\Gamma = 10^{-4}$.

$\Delta\phi$ the width of this antiresonance is determined either by $k_B T$, as in the present regime $eV_T \ll k_B T \ll |eV|$ (black and red curves in Fig. 2(a)), or by eV_T , in the regime $k_B T \ll eV_T \ll |eV|$. It is important to note that this antiresonance appears when $|\eta_2| \neq 0$ and $\Delta\phi \neq 0$ and does not arise when the QD is effectively coupled to a single MBS, that is for $\Delta\phi = 0$ or $|\eta_2| = 0$. Note also, that a difference in several orders of magnitude between the corresponding energy scales mentioned above is crucial for its appearance. Indeed, if this difference was only one order of magnitude or less, the antiresonance would be strongly suppressed because the resonances located at $\hbar\omega = 0$ and $\hbar\omega = -|eV|$ (see Ref. [96]) would overlap and fully wash out the antiresonance at $\hbar\omega = -|eV|/2$. However, when the energy scales are separated by several orders of magnitude, as in the present case, the resonances located at $\hbar\omega = 0$ and $\hbar\omega = -|eV|$ are far away from each other and there emerges the antiresonance at $\hbar\omega = -|eV|/2$ shown in Fig. 2. The minimum of this antiresonance is located exactly at $\hbar\omega = -|eV|/2$. Both its amplitude and width depend on $\Delta\phi$. The amplitude of the antiresonance first grows with $\Delta\phi$, reaches a maximal value at an intermediate value of $\Delta\phi$ (see Fig. 2(a)), and after that decreases to a small but finite value when the Majorana phase difference goes to $\Delta\phi = \pi/2$ (see Fig. 2(b)). In contrast, as can be seen from Figs. 2(a) and (b), the width of the emission antiresonance always grows with $\Delta\phi$ from a value of the order of $k_B T$, at small values of $\Delta\phi$, to very large values, about $10^2 k_B T$, at $\Delta\phi = \pi/2$. The appearance of this antiresonance qualitatively changes the behavior of the differential thermoelectric quantum noise. Indeed, we find that

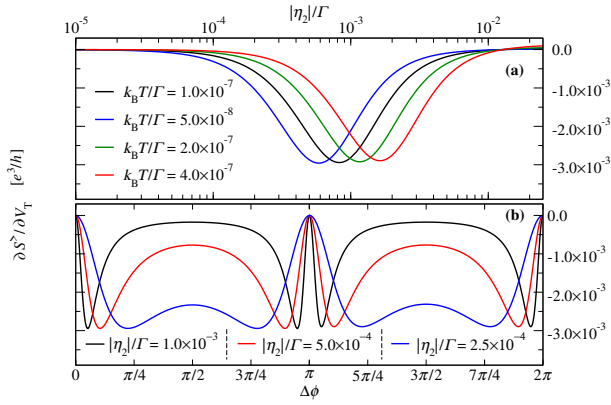


FIG. 3. Differential thermoelectric quantum noise, $\partial S^>(\omega, V, V_T, \Delta\phi)/\partial V_T$, at $\hbar\omega = -|eV|/2$. Panel (a): As a function of $|\eta_2|$ for $\Delta\phi = \pi/16$ and four values of the temperature $k_B T$. Specifically, $k_B T/\Gamma = 10^{-7}$ (black), $k_B T/\Gamma = 5.0 \times 10^{-8}$ (blue), $k_B T/\Gamma = 2.0 \times 10^{-7}$ (green), $k_B T/\Gamma = 4.0 \times 10^{-7}$ (red). Panel (b): As a function of $\Delta\phi$ for $k_B T/\Gamma = 10^{-7}$ and three values of $|\eta_2|$. Specifically, $|\eta_2|/\Gamma = 1.0 \times 10^{-3}$ (black), $|\eta_2|/\Gamma = 5.0 \times 10^{-4}$ (red), $|\eta_2|/\Gamma = 2.5 \times 10^{-4}$ (blue). The other parameters are the same as in Fig. 2.

in the absorption spectra ($\omega > 0$) there does not arise an antiresonance at $\hbar\omega = |eV|/2$ which could have been the absorption partner of the emission antiresonance. As a result, $\partial S^>(\omega, V, V_T, \Delta\phi)/\partial V_T$ loses its symmetry in ω and the emission and absorption spectra are in general not related to each other. This is in contrast to the symmetric differential thermoelectric quantum noise observed in Ref. [96] for the case $|\eta_2| = 0$.

To further analyze the behavior of the emission antiresonance we have calculated the differential thermoelectric quantum noise at $\hbar\omega = -|eV|/2$ as a function of $|\eta_2|$ and $\Delta\phi$ for different temperatures as shown in Fig. 3. From the dependence on the Majorana tunneling amplitude $|\eta_2|$, demonstrated in Fig. 3(a), one can see that the curves for different temperatures are characterized by a minimum where the amplitude of the emission antiresonance is maximal. The minima of all the curves are almost the same. This means that the maximal amplitude of the emission antiresonance weakly depends on the temperature whose effect is just to shift it to another value of $|\eta_2|$. To physically interpret such a shift, it is important to note that thermal fluctuations represent a mechanism suppressing the Majorana interference. Therefore they will compete against the fluctuations induced by the interfering MBSs when $|\eta_2| \neq 0$ and $\Delta\phi \neq 0$. Indeed, as demonstrated in Fig. 3(a), when the temperature grows, thermal fluctuations push out the emission antiresonance from weak to strong Majorana interference, that is from smaller to larger values of $|\eta_2|$. Thus, in order to restore this antiresonance after it has been destroyed by thermal fluctuations, one has to increase $|\eta_2|$ to enhance the fluctuations induced by the Majorana interference. However, the increase of $|\eta_2|$ should not be too large since

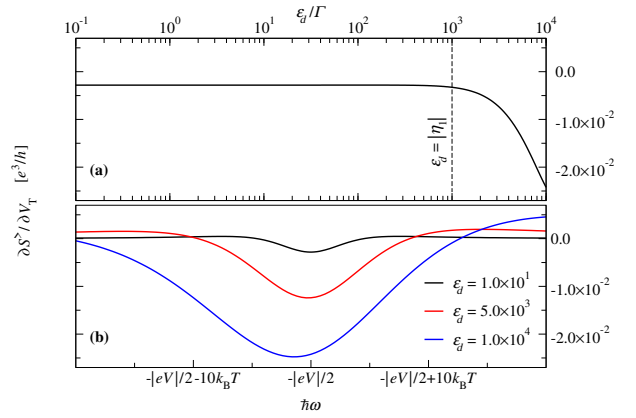


FIG. 4. Differential thermoelectric quantum noise, $\partial S^>(\omega, V, V_T, \Delta\phi)/\partial V_T$, in the emission domain ($\omega < 0$). Panel (a): As a function of the gate voltage ϵ_d at the frequency $\hbar\omega = -|eV|/2$. Panel (b): As a function of the frequency $\hbar\omega$ in a vicinity of $\hbar\omega = -|eV|/2$ for various values of the gate voltage ϵ_d . Specifically, $\epsilon_d/\Gamma = 10$ (black), $\epsilon_d/\Gamma = 5.0 \times 10^3$ (red), $\epsilon_d/\Gamma = 10^4$ (blue). In both panels $\Delta\phi = \pi/16$. The other parameters are the same as in Fig. 2.

very strong interference becomes destructive and, as can be seen in Fig. 3(a), ruins the antiresonance. Note also, that larger values of $|\eta_2|$ shrink the range of $\Delta\phi$ where the amplitude of the emission antiresonance is large enough to be observed in experiments. This may be seen from the black curve in Fig. 3(b). At the same time the blue curve in Fig. 3(b) shows that for smaller values of $|\eta_2|$ the amplitude of the emission antiresonance becomes larger in a wide range of $\Delta\phi$. Since for $\Delta\phi = 0, \pi$ the QD is effectively coupled to a single MBS, the emission antiresonance is absent at $\Delta\phi = 0, \pi$ for any finite value of $|\eta_2|$ and its amplitude is strongly suppressed in vicinities of these points. In the limit $|\eta_2| \rightarrow 0$ these vicinities will widen indicating the disappearance of the Majorana interference for any finite value of $\Delta\phi$.

Let us look how the results shown above change when one moves outside the universal Majorana regime (see Eq. (40)) as may happen during possible experiments. As has been mentioned above, within the universal Majorana regime the differential thermoelectric quantum noise is independent of the gate voltage. This may be seen from Fig. 4(a), which shows $\partial S^>(\omega, V, V_T, \Delta\phi)/\partial V_T$ as a function of the gate voltage ϵ_d at the minimum of the emission antiresonance, that is at $\hbar\omega = -|eV|/2$. As can be seen, the minimum of the emission antiresonance is independent of ϵ_d for gate voltages satisfying the condition in Eq. (40), $\epsilon_d < |\eta_1|$. Weak deviations start to appear when $\epsilon_d \sim |\eta_1|$. For larger gate voltages, $\epsilon_d > |\eta_1|$, the minimum of the emission antiresonance acquires a strong dependence on ϵ_d . The same is also true at other frequencies so that the whole antiresonance remains unchanged when ϵ_d is varied within its upper bound, $\epsilon_d < |\eta_1|$. It turns out that for larger gate voltages, $\epsilon_d > |\eta_1|$, the emission antiresonance is still present in a vicinity of the

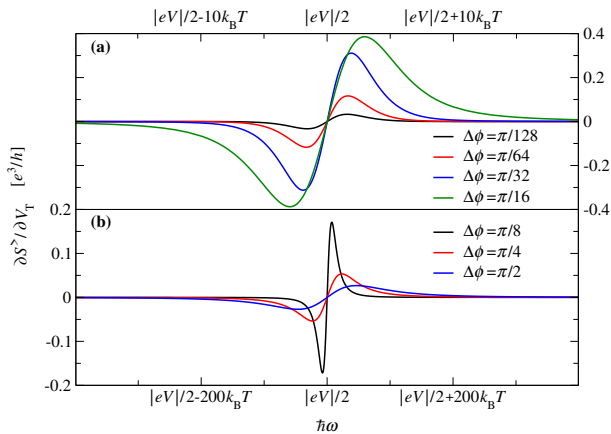


FIG. 5. Frequency dependence of the differential thermoelectric quantum noise, $\partial S^>(\omega, V, V_T, \Delta\phi)/\partial V_T$, in a vicinity of the frequency $\hbar\omega = |eV|/2$ (absorption noise, domain $\omega > 0$) for small bias voltages, $|eV| \ll \Gamma$, and for various values of the Majorana tunneling phase difference $\Delta\phi$. Specifically, for all the curves $|eV|/\Gamma = 10^{-2}$ and, in Panel (a), $\Delta\phi = \pi/128$ (black), $\Delta\phi = \pi/64$ (red), $\Delta\phi = \pi/32$ (blue), $\Delta\phi = \pi/16$ (green), in Panel (b), $\Delta\phi = \pi/8$ (black), $\Delta\phi = \pi/4$ (red), $\Delta\phi = \pi/2$ (blue). The other parameters have the same values as in Fig. 2.

frequency $\hbar\omega = -|eV|/2$. However, as demonstrated by Fig. 4(b), when ϵ_d starts to exceed $|\eta_1|$, the emission antiresonance acquires two qualitative changes. First, its minimum shifts from $\hbar\omega = -|eV|/2$. Second, it becomes asymmetric with respect to its minimum. Both the shift of the minimum and asymmetry get larger and larger as ϵ_d more and more exceeds $|\eta_1|$ as can be seen from the red and blue curves in Fig. 4(b). Additionally, the antiresonance exhibits quantitative changes, namely, its amplitude and width significantly increase which might facilitate its experimental detection.

The behavior of the absorption noise ($\omega > 0$) in the vicinity of the frequency $\hbar\omega = |eV|/2$ turns out to be qualitatively different from the emission noise ($\omega < 0$) in the vicinity of the frequency $\hbar\omega = -|eV|/2$. When the QD is effectively coupled to a single MBS, that is when $|\eta_2| = 0$ or $\Delta\phi = 0$, the differential thermoelectric quantum noise is strongly suppressed in the vicinity of the frequency $\hbar\omega = |eV|/2$ and the absorption spectra are characterized by the resonance at $\hbar\omega = |eV|$ as discussed in Ref. [96]. However, for finite values of $|\eta_2|$ the differential thermoelectric quantum noise in the vicinity of $\hbar\omega = |eV|/2$ becomes finite when one increases the Majorana tunneling phase difference $\Delta\phi$ from zero to finite values. Indeed, Fig. 5(a) shows that for small values of $\Delta\phi$ there develops an antiresonance-resonance pair whose center is located exactly at $\hbar\omega = |eV|/2$. To be more specific, $\partial S^>(\omega, V, V_T, \Delta\phi)/\partial V_T = 0$ at the frequency $\hbar\omega = |eV|/2$ and reaches a negative minimum and positive maximum with equal amplitudes at some frequencies $\hbar\omega_{min} < |eV|/2$ and $\hbar\omega_{max} > |eV|/2$, respectively. The frequencies $\hbar\omega_{min}$ and $\hbar\omega_{max}$ are equidistant from the

center of the antiresonance-resonance pair, that is from the frequency $\hbar\omega = |eV|/2$. For small values of $\Delta\phi$ the amplitudes of the antiresonance and resonance are also small (see the black and red curves with $\Delta\phi = \pi/128$ and $\Delta\phi = \pi/64$) and their widths are of the order of the temperature $k_B T$. For larger values of $\Delta\phi$ (see the green curve with $\Delta\phi = \pi/16$) the amplitudes of the antiresonance and resonance quickly grow. Their widths increase almost one order of magnitude so that their extension in the frequency domain is almost $10k_B T$. However, after their increase the amplitudes of the antiresonance and resonance start to decrease at some value of $\Delta\phi$ and are significantly reduced when the Majorana tunneling phase difference approaches the value $\Delta\phi = \pi/2$ as demonstrated in Fig. 5(b). In contrast, their widths continue to grow and their extension in the frequency domain becomes very large, about $10^2 k_B T$ (see the blue curve with $\Delta\phi = \pi/2$). Similar to the emission antiresonance the absorption antiresonance-resonance pair is of pure Majorana interference nature because it is strongly suppressed when the QD is effectively coupled to a single MBS that is when $|\eta_2| = 0$ or $\Delta\phi = 0$ and, as mentioned above, the emission and absorption spectra are symmetrically related [96]. However, when $|\eta_2| \neq 0$ and $\Delta\phi \neq 0$, the behavior of $\partial S^>(\omega, V, V_T, \Delta\phi)/\partial V_T$ in the domains $\omega < 0$ and $\omega > 0$ is qualitatively different at small bias voltages, $|eV| \ll \Gamma$, and the emission and absorption spectra are not related to each other. This situation changes for large bias voltages, $|eV| \gg \Gamma$, as will be shown below.

At large bias voltages, $|eV| \gg \Gamma$, it turns out that the differential thermoelectric quantum noise is suppressed at all frequencies except for vicinities of the frequencies $\hbar\omega = \pm|eV|/2$. In particular, when the bias voltage is increased to large values, $|eV| \gg \Gamma$, the absorption antiresonance-resonance pair discussed above in the regime $|eV| \ll \Gamma$ (see Fig. 5) is retained at $\hbar\omega = |eV|/2$ but, as we find numerically, the amplitudes of the antiresonance and resonance are reduced exactly twice in the regime $|eV| \gg \Gamma$ as can be seen in Fig. 6. This happens for all values of the Majorana tunneling phase difference $\Delta\phi$. The behavior of the widths of the antiresonance and resonance in the regime $|eV| \gg \Gamma$ is the same as in the regime $|eV| \ll \Gamma$. Specifically, for small values of $\Delta\phi$ the widths are of the order of the temperature $k_B T$ (black and red curves in Fig. 6(a)), for larger values of $\Delta\phi$ the antiresonance and resonance widen up to $10k_B T$ (blue curve in Fig. 6(a)) whereas for $\Delta\phi = \pi/2$ (blue curve in Fig. 6(b)) their widths are maximal, about $10^2 k_B T$ in the frequency domain. Turning to the emission spectra, our numerical calculations reveal that when the bias voltage is increased, the emission antiresonance observed in the regime $|eV| \ll \Gamma$ (see Figs. 2 and 3) transforms into a pair antiresonance-resonance located at the frequency $\hbar\omega = -|eV|/2$. It turns out that in the regime of large bias voltages, $|eV| \gg \Gamma$, this emission antiresonance-resonance pair is fully identical to the absorption antiresonance-resonance pair at any value of the Majorana tunneling phase difference $\Delta\phi$ as demonstrated

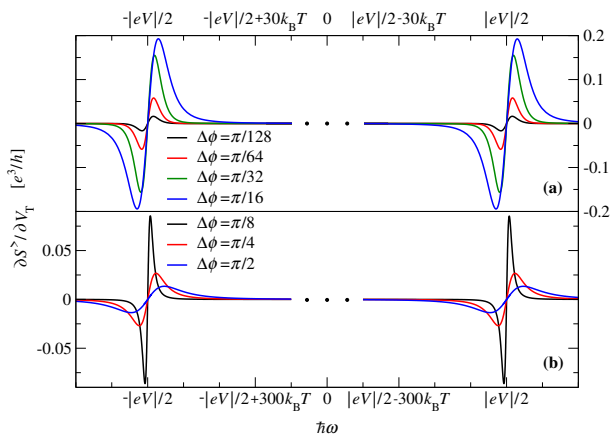


FIG. 6. Frequency dependence of the differential thermoelectric quantum noise, $\partial S^>(\omega, V, V_T, \Delta\phi)/\partial V_T$, in the vicinity of the two frequencies, $\hbar\omega = -|eV|/2$ (emission noise, domain $\omega < 0$) and $\hbar\omega = |eV|/2$ (absorption noise, domain $\omega > 0$), for large bias voltages, $|eV| \gg \Gamma$, and for various values of the Majorana tunneling phase difference $\Delta\phi$. Specifically, for all the curves $|eV|/\Gamma = 10^2$ and, in Panel (a), $\Delta\phi = \pi/128$ (black), $\Delta\phi = \pi/64$ (red), $\Delta\phi = \pi/32$ (green), $\Delta\phi = \pi/16$ (blue), in Panel (b), $\Delta\phi = \pi/8$ (black), $\Delta\phi = \pi/4$ (red), $\Delta\phi = \pi/2$ (blue). The other parameters have the same values as in Fig. 2.

in Figs. 6(a) and (b). Note that both the emission and absorption antiresonance-resonance pairs are of pure Majorana interference nature because both of them appear only at finite values of $|\eta_2|$ and $\Delta\phi$ whereas for $|\eta_2| = 0$ or $\Delta\phi = 0$, when the QD is effectively coupled to a single MBS, the differential thermoelectric quantum noise is suppressed at all frequencies for $|eV| \gg \Gamma$. Since the absorption and emission antiresonance-resonance pairs are identical, we conclude that at large bias voltages, $|eV| \gg \Gamma$, the Majorana interference makes the differential thermoelectric quantum noise antisymmetric with respect to the frequency ω , that is

$$\frac{\partial S^>(-\omega, V, V_T, \Delta\phi)}{\partial V_T} = -\frac{\partial S^>(\omega, V, V_T, \Delta\phi)}{\partial V_T}, \quad (41)$$

$$k_B T \ll \Gamma, \quad |eV| \gg \Gamma, \quad 0 \leq \Delta\phi < 2\pi.$$

Thus it is the interplay of the Majorana interference and strong nonequilibrium which establishes the antisymmetric relation, expressed by Eq. (41), between the absorption and emission spectra of the differential thermoelectric quantum noise.

At this point a qualitative physical explanation of the numerical results would be appropriate. Particularly, it would be useful to try to understand why the emission and absorption spectra are different at small bias voltages, $|eV| \ll \Gamma$, and become similar at large bias voltages, $|eV| \gg \Gamma$. To this end, we note that the behavior of the differential thermoelectric quantum noise in vicinities of $\hbar\omega = \mp|eV|/2$ is governed by two tunneling processes. The first one is from the TS to the left metallic contact and it is this process which is responsible for the emis-

sion spectra arising around $\hbar\omega = -|eV|/2$. The second process is the tunneling from the left contact to the TS, and it is responsible for the absorption spectra arising around $\hbar\omega = |eV|/2$. An emission of a photon with an energy $\hbar\omega \sim |eV|/2$ decreases the energy of a quasiparticle and it goes from the zero energy in the TS to a negative energy in a vicinity of the chemical potential of the left contact. An absorption of a photon with an energy $\hbar\omega \sim |eV|/2$ increases the energy of a quasiparticle and it goes from a negative energy in a vicinity of the chemical potential of the left contact to the zero energy in the TS. Note, that we consider emission or absorption tunneling processes which, respectively, end in or originate from the vicinity of width $k_B T$ around the chemical potential of the left contact, $\mu_L = -|eV|/2$, because we consider the differential thermoelectric quantum noise. It is given as the derivative over V_T which is finite only within the vicinity of width $k_B T$ around $\hbar\omega = -|eV|/2$ or $\hbar\omega = |eV|/2$ for, respectively, emission or absorption processes. The difference between the emission and absorption spectra for the case of small bias voltages, $|eV| \ll \Gamma$, may be qualitatively understood if we take into account that the two tunneling processes mentioned above occur via the QD and thus involve the nonequilibrium distribution function, $n_d(\epsilon)$, of the QD. Since the QD is non-interacting, its distribution function is of the double step form (see Ref. [106]), $n_d(\epsilon) = [n_L(\epsilon) + n_R(\epsilon)]/2$. More specifically, since the differential thermoelectric quantum noise is given by the derivative over V_T , the QD distribution function $n_d(\epsilon)$ contributes to an emission or absorption process through the thermally broadened region of $n_L(\epsilon)/2$, that is again in the vicinity of width $k_B T$ around $\hbar\omega = -|eV|/2$ or $\hbar\omega = |eV|/2$, respectively. Note, that the zero energy level of the QD is induced by MBSs and is broadened by the coupling to the contacts. Its width is given by Γ . Thus the thermally broadened region of $n_d(\epsilon)$, namely the vicinity of μ_L of width $k_B T$, is fully within the width Γ of the QD zero energy level when $|eV| \ll \Gamma$ and it participates in an emission and absorption tunneling process through the factors $n_d(\epsilon)$, $[1 - n_d(\epsilon)]$ combined with the factors $n_L(\epsilon)$, $[1 - n_L(\epsilon)]$. These combinations are different for emission and absorption processes which qualitatively explains the difference between, respectively, the emission and absorption spectra obtained after integrating these combinations over the energy domain. Now, turning to the case of large bias voltages, $|eV| \gg \Gamma$, we note that the derivative of the QD distribution function $n_d(\epsilon)$ over V_T does not contribute anymore to the differential thermoelectric quantum noise $\partial S^>(\omega, V, V_T, \Delta\phi)/\partial V_T$ because the thermally broadened region of $n_d(\epsilon)$ around μ_L is fully outside the width Γ of the QD zero energy level when $|eV| \gg \Gamma$. Instead, the factors $n_d(\epsilon)$, $[1 - n_d(\epsilon)]$ become equal, $n_d(\epsilon) = 1 - n_d(\epsilon) = 1/2$, over the whole width Γ of the QD zero energy level for $|eV| \gg \Gamma$ and their combinations with the factors $n_L(\epsilon)$, $[1 - n_L(\epsilon)]$ result in similar emission and absorption spectra obtained after integrations in the energy domain. Moreover, since the

contribution from the derivative of $n_d(\epsilon)$ over V_T is similar to the contribution of the derivative of $n_L(\epsilon)$ over V_T , it looks plausible that the disappearance of the former contribution to the derivative $\partial S^>(\omega, V, V_T, \Delta\phi)/\partial V_T$ in the regime $|eV| \gg \Gamma$ reduces the amplitudes of the antiresonance-resonance pairs twice in comparison with the regime $|eV| \ll \Gamma$.

We would like to emphasize that the explanation given above is rather qualitative. In particular, it can help to understand why in the regime of small bias voltages, $|eV| \ll \Gamma$, the emission and absorption spectra are different and why they are similar in the regime of large bias voltages, $|eV| \gg \Gamma$, but it cannot explain the exact shape of the spectra. For example, it does not explain why in the regime of small bias voltages there develops an antiresonance in the emission spectra and an antiresonance-resonance pair in the absorption spectra. To understand where these shapes come from it is important to note that the role of the MBSs is not only in the appearance of the zero energy level in the QD but also in the emergence of a strong energy dependence of the density of states $\nu_d(\epsilon)$ in the QD at low energies. This energy dependence is the result of the Majorana interference which, on one side, strongly suppresses the density of states at low energies but, on the other side, it results in the appearance of wide regions where various derivatives of the density of states essentially increase. The results presented above reveal that for $|\eta_2| \neq 0$ and $\Delta\phi \neq 0$ the magnitude of these derivatives and the size of the regions where they are sufficiently large essentially determine the behavior of the differential thermoelectric quantum noise specified as the derivative over V_T . In fact, a complex interplay between the thermoelectric nonequilibrium and Majorana interference arises within and outside the thermally broadened region of $n_L(\epsilon)$. For example, outside this region the fluctuation response of quasiparticles to the thermal voltage V_T would be strongly suppressed for $|\eta_2| = 0$ or $\Delta\phi = 0$ as expressed by the exponential decay of the derivative of $n_L(\epsilon)$ over V_T outside the domain of width $k_B T$ around μ_L . However, for $|\eta_2| \neq 0$ and $\Delta\phi \neq 0$ the region where derivatives of $\nu_d(\epsilon)$ are sufficiently large may become wider than the thermally broadened region of $n_L(\epsilon)$. In this situation the corresponding factors, derivatives of $\nu_d(\epsilon)$ over ϵ and the derivative of $n_L(\epsilon)$ over V_T , start to compete. It is this competition between the Majorana interference and thermoelectric nonequilibrium which results in specific shapes of the emission and absorption spectra within and outside the thermally broadened region of $n_L(\epsilon)$. To support our reasoning, we show in Fig. 7 the QD density of states (Fig. 7(a)), its first (Fig. 7(b)) and second (Fig. 7(c)) derivatives over the energy. Comparing the shape of the curves in Fig. 2 with the shape of the curve in Fig. 7(c) as well as comparing Fig. 5 with Fig. 7(b), we see that the difference between the emission and absorption spectra is quantitatively rooted in the fact that in the regime of small bias voltages, $|eV| \ll \Gamma$, the emission spectra are governed by the second derivative of the QD density of

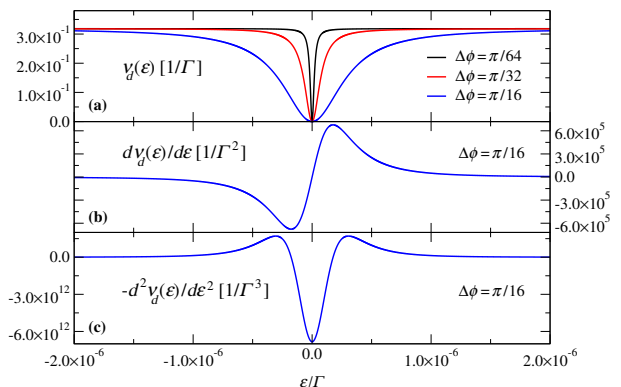


FIG. 7. Panel (a): Density of states of the QD, $\nu_d(\epsilon)$, for $\Delta\phi = \pi/64$ (black), $\Delta\phi = \pi/32$ (red), $\Delta\phi = \pi/16$ (blue). Panel (b): First derivative of the density of states, $d\nu_d(\epsilon)/d\epsilon$, for $\Delta\phi = \pi/16$. Panel (c): Second derivative of the density of states, $-d^2\nu_d(\epsilon)/d\epsilon^2$, for $\Delta\phi = \pi/16$. In all the panels $\epsilon_d/\Gamma = 10$, $|\eta_1|/\Gamma = 10^3$, $|\eta_2|/\Gamma = 10^{-3}$, $\xi/\Gamma = 10^{-4}$.

states, $-d^2\nu_d(\epsilon)/d\epsilon^2$, whereas the absorption spectra are governed by its first derivative, $d\nu_d(\epsilon)/d\epsilon$. We also see that for large bias voltages, $|eV| \gg \Gamma$, the emission and absorption spectra shown in Fig. 6 are both governed by the first derivative $d\nu_d(\epsilon)/d\epsilon$ of the QD density of states shown in Fig. 7(b). Note also, that the derivatives shown in Figs. 7(b) and (c) are huge and thus are able to compete with the exponential decay of the derivative of $n_L(\epsilon)$ over V_T outside the thermally broadened region to produce values of $\partial S^>(\omega, V, V_T, \Delta\phi)/\partial V_T$ which would be sufficiently large for an experimental detection.

Let us recall that the results presented above have been obtained in the regime specified by $eV_T \ll k_B T \ll |eV| < |\eta_1|$. Within this regime we have analyzed the two cases, $|eV| \ll \Gamma$ and $|eV| \gg \Gamma$. So, the upper bound for the temperature is always the bias voltage. Specifically, $k_B T$ should be at least one order of magnitude less than $|eV|$. In turn, the upper bound for the bias voltage is always $|\eta_1|$. The above two cases are characterized by low temperatures, $k_B T \ll \Gamma$. The third case within the regime $eV_T \ll k_B T \ll |eV| < |\eta_1|$ is specified by high temperatures, $k_B T \gg \Gamma$, and is analyzed below.

It turns out that the antisymmetric relation between the absorption and emission spectra, Eq. (41), arises in strong nonequilibrium also when the QD is effectively coupled to a single MBS, that is when $|\eta_2| = 0$ or $\Delta\phi = 0$. This happens in the regime of high temperatures, $k_B T \gg \Gamma$, as demonstrated by the black curve in Fig. 8(a) or (b) for which $\Delta\phi = 0$. In this case the two MBSs do not interfere with different tunneling phases but $\partial S^>(\omega, V, V_T, \Delta\phi)/\partial V_T$ is not suppressed at all frequencies as has been observed above in the regime of low temperatures, $k_B T \ll \Gamma$. Indeed, at high temperatures there arise thermally excited Majorana resonance-antiresonance pairs. They have a non-interfering nature and are located at $\hbar\omega = \pm|eV|/2$ in the absorption and emission spectra, respectively. When the interference of

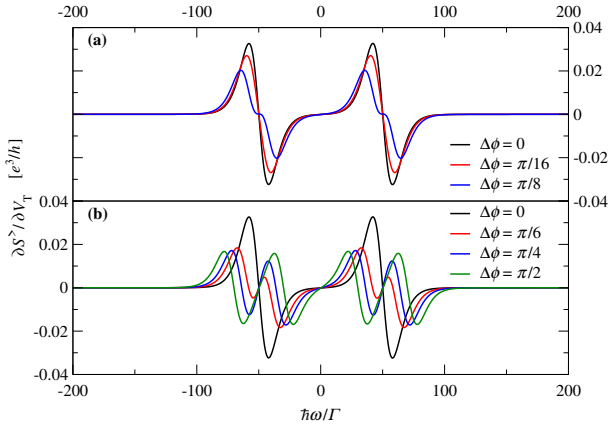


FIG. 8. Frequency dependence of the differential thermoelectric quantum noise, $\partial S^>(\omega, V, V_T, \Delta\phi)/\partial V_T$, in the emission ($\omega < 0$) and absorption ($\omega > 0$) domains for large bias voltages and temperatures, $|eV| \gg \Gamma$, $k_B T \gg \Gamma$, and for various values of the Majorana tunneling phase difference $\Delta\phi$. Specifically, for all the curves $|eV|/\Gamma = 10^2$, $k_B T/\Gamma = 5.0$ and, in Panel (a), $\Delta\phi = 0$ (black), $\Delta\phi = \pi/16$ (red), $\Delta\phi = \pi/8$ (blue), in Panel (b), $\Delta\phi = 0$ (black), $\Delta\phi = \pi/6$ (red), $\Delta\phi = \pi/4$ (blue), $\Delta\phi = \pi/2$ (green). The values of the other parameters: $\epsilon_d/\Gamma = 10$, $eV_T/\Gamma = 10^{-3}$, $|\eta_1|/\Gamma = 2.5 \times 10^2$, $|\eta_2|/\Gamma = 10$, $\xi/\Gamma = 10^{-4}$.

the two MBSs with different tunneling phases is gradually switched on by increasing $\Delta\phi$ at a finite value of $|\eta_2|$, the amplitudes of the thermal resonance and antiresonance start to decrease as can be seen from the red curve with $\Delta\phi = \pi/16$ in Fig. 8(a). Further increase of $\Delta\phi$ produces a notable reduction of the negative slopes in small vicinities of $\hbar\omega = \pm|eV|/2$ (blue curve with $\Delta\phi = \pi/8$ in Fig. 8(a)) which is a precursor to the formation of the Majorana interference induced antiresonance-resonance pairs. For larger values of $\Delta\phi$ the Majorana interference pattern fully develops. Indeed, as demonstrated in Fig. 8(b), in the centers of the thermally excited pairs resonance-antiresonance there emerge pairs antiresonance-resonance induced by the Majorana interference. This is clearly seen by comparing the black curve, corresponding to the system with the QD effectively coupled to a single MBS ($\Delta\phi = 0$), with the red ($\Delta\phi = \pi/6$), blue ($\Delta\phi = \pi/4$) and green ($\Delta\phi = \pi/2$) curves, corresponding to the system where the two MBSs interfere with different tunneling phases. Note, that for $\Delta\phi = \pi/2$ the Majorana interference becomes so strong that the amplitudes of the antiresonance and resonance in the Majorana interference induced pairs antiresonance-resonance are almost equal to the ones in the thermally excited pairs resonance-antiresonance. What is important to note is that the Majorana interference does not break the original (at $\Delta\phi = 0$) antisymmetric character of the differential thermoelectric quantum noise composed in the absence of the Majorana interference of the two thermally excited pairs resonance-antiresonance. Indeed, the absorption and

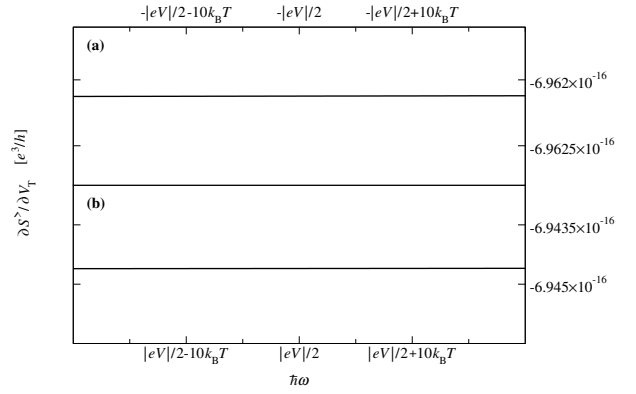


FIG. 9. Frequency dependence of the differential thermoelectric quantum noise, $\partial S^>(\omega, V, V_T, \Delta\phi)/\partial V_T$, for ABSs. Panels (a) and (b) show, respectively, the emission ($\omega < 0$) and absorption ($\omega > 0$) domains in the vicinities of $\hbar\omega = \mp|eV|/2$ in the same regime of small temperatures and bias voltages as the one used for Figs. 2 and 5 for the case of MBSs. Here $|\eta_2|/\Gamma = 5.0 \times 10^2$, $\xi/\Gamma = 10^2$ and $\Delta\phi = \pi/16$. The values of the other parameters are the same as in Fig. 2.

emission antiresonance-resonance pairs induced by the Majorana interference in the centers of the corresponding thermally excited resonance-antiresonance pairs are fully identical. Therefore, in the regime of high temperatures, $k_B T \gg \Gamma$, the differential thermoelectric quantum noise is also antisymmetric,

$$\frac{\partial S^>(-\omega, V, V_T, \Delta\phi)}{\partial V_T} = -\frac{\partial S^>(\omega, V, V_T, \Delta\phi)}{\partial V_T}, \quad (42)$$

$$k_B T \gg \Gamma, \quad |eV| \gg \Gamma, \quad 0 \leq \Delta\phi < 2\pi.$$

However, in this case the antisymmetry is produced by an interplay of highly nonequilibrium states and thermal fluctuations whereas the Majorana interference, when sufficiently strong, introduces characteristic antiresonance-resonance pairs without breaking the antisymmetric relation between the absorption and emission spectra. The picture described above qualitatively changes when MBSs are replaced with ABSs as discussed below.

To analyze the differential thermoelectric quantum noise resulting from ABSs coupled to the QD and compare its behavior with the one discussed above for the QD interacting with MBSs one may apply our model in a suitable regime. Namely, the QD interacting with ABSs may be modeled (see Refs. [94, 102]) by using a large value of the overlap energy ξ and a value of the second Majorana tunneling amplitude $|\eta_2|$ of the same order as the value of the first one, that is $|\eta_2| \sim |\eta_1|$. In the low temperature regime both for small ($|eV| \ll \Gamma$) and large ($|eV| \gg \Gamma$) bias voltages the differential thermoelectric quantum noise induced by ABSs turns out to be strongly suppressed in vicinities of the frequencies $\hbar\omega = \mp|eV|/2$. For example, Figs. 9(a) and (b) show $\partial S^>(\omega, V, V_T, \Delta\phi)/\partial V_T$ for ABSs in the vicinities of, respectively, $\hbar\omega = \mp|eV|/2$ for $|eV| \ll \Gamma$, where in the case

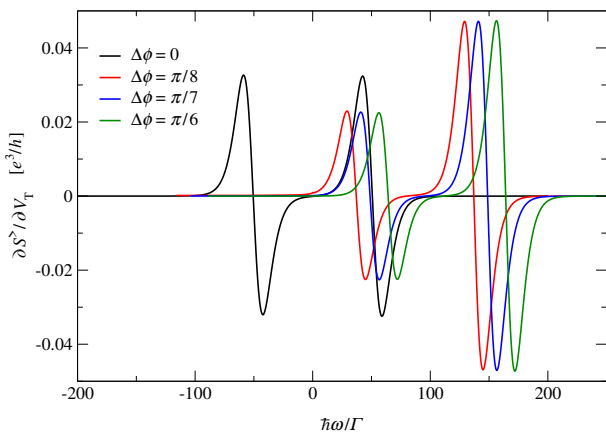


FIG. 10. Frequency dependence of the differential thermoelectric quantum noise, $\partial S^>(\omega, V, V_T, \Delta\phi)/\partial V_T$, for ABSs. The emission ($\omega < 0$) and absorption ($\omega > 0$) domains are shown in the regime of large bias voltages and temperatures, $|eV| \gg \Gamma$, $k_B T \gg \Gamma$, for various values of the tunneling phase difference $\Delta\phi$. Specifically, for all the curves $|eV|/\Gamma = 10^2$, $k_B T/\Gamma = 5.0$ and $\Delta\phi = 0$ (black), $\Delta\phi = \pi/8$ (red), $\Delta\phi = \pi/7$ (blue), $\Delta\phi = \pi/6$ (green). The values of the other parameters: $\epsilon_d/\Gamma = 10$, $eV_T/\Gamma = 10^{-3}$, $|\eta_1|/\Gamma = 2.5 \times 10^2$, $|\eta_2|/\Gamma = 1.25 \times 10^2$, $\xi/\Gamma = 10^2$.

of MBSs there appear the emission antiresonance shown in Fig. 2 in the vicinity of the frequency $\hbar\omega = -|eV|/2$ and the absorption antiresonance-resonance pair shown in Fig. 5 in the vicinity of the frequency $\hbar\omega = |eV|/2$. As we can see from Figs. 9(a) and (b), the differential thermoelectric quantum noise induced by ABSs in the regime of low temperatures and small bias voltages is suppressed several orders of magnitude in comparison with the case of MBSs and does not exhibit any emission antiresonance and absorption antiresonance-resonance pair. Additionally, within the low temperature regime, the differential thermoelectric quantum noise induced by ABSs turns out to be strongly suppressed around the frequencies $\hbar\omega = \mp|eV|/2$ also for large bias voltages, $|eV| \gg \Gamma$, and, in contrast to the case of MBSs (see Fig. 6), does not exhibit any antiresonance-resonance pair for any value of $\Delta\phi$. In the high temperature regime the behavior of the differential thermoelectric quantum noise induced by ABSs is shown in Fig. 10. Comparing it with the one discussed above for MBSs in Fig. 8 one explicitly observes an exceptional role of the Majorana interference. Indeed, as we can see, for $\Delta\phi = 0$ the black curve in Fig. 8(a) or (b) and the black curve in Fig. 10 are identical. This means that when the QD is effectively coupled to a single MBS, the differential thermoelectric quantum noise in the regime of large bias voltages and temperatures, $|eV| \gg \Gamma$, $k_B T \gg \Gamma$, would not be able to distinguish this single MBS from ABSs. Remarkably, when $\Delta\phi \neq 0$, interference effects reveal a fundamental difference between fluctuation responses of the two MBSs with different tunneling phases and ABSs making the differential thermoelectric quantum noise of ABSs

qualitatively different from the one characterizing MBSs. Indeed, as one can see in Fig. 10, finite values of $\Delta\phi$ do not produce any pairs antiresonance-resonance in the centers of the thermally excited resonance-antiresonance pairs as it happens for the system with the MBSs (see Fig. 8). This is clearly seen in the red, blue and green curves with $\Delta\phi = \pi/8$, $\Delta\phi = \pi/7$ and $\Delta\phi = \pi/6$, respectively. Instead, Fig. 10 shows that the thermally excited pairs resonance-antiresonance shift to positive frequencies, that is to the absorption spectra. Additionally, the amplitudes of the resonance and antiresonance in the pair located at a larger frequency increase whereas those in the pair located at a smaller frequency decrease. As a result, we see that for ABSs the differential thermoelectric quantum noise loses its antisymmetry as a function of the frequency ω , that is

$$\frac{\partial S^>(-\omega, V, V_T, \Delta\phi)}{\partial V_T} \neq -\frac{\partial S^>(\omega, V, V_T, \Delta\phi)}{\partial V_T}, \quad (43)$$

$$\Delta\phi \neq 0.$$

Therefore, we conclude that in the high temperature regime exactly the interference behavior of the differential thermoelectric quantum noise, emerging for $\Delta\phi \neq 0$, enables one to explicitly and qualitatively distinguish systems with MBSs from those where fluctuations of thermoelectric currents are governed by ABSs.

V. CONCLUSION

In conclusion, we have analyzed fluctuations of thermoelectric currents flowing through a nonequilibrium QD interacting with MBSs. Particularly, we have focused on the differential thermoelectric quantum noise, $\partial S^>(\omega, V, V_T, \Delta\phi)/\partial V_T$, which results from an interplay between Majorana interference effects induced by the phase difference $\Delta\phi$ and nonequilibrium states produced by both electric and thermal voltages, V and V_T , respectively, at finite frequencies ω . In the regime of low bias voltages we have found an emission ($\omega < 0$) antiresonance located at $\hbar\omega = -|eV|/2$. On the absorption ($\omega > 0$) side of the spectra we have found an antiresonance-resonance pair with its center at $\hbar\omega = |eV|/2$. The minimum and maximum of the antiresonance and resonance are symmetrically located with respect to the frequency $\hbar\omega = |eV|/2$ and have equal amplitudes. Both the emission antiresonance and absorption antiresonance-resonance pair involve the Majorana modes with $\Delta\phi \neq 0$ and thus turn out to be of pure Majorana interference nature. In the regime of large bias voltages it has been found that the absorption antiresonance-resonance pair persists but the amplitudes of the antiresonance and resonance are reduced exactly twice. At the same time, the emission antiresonance disappears in the regime of large bias voltages and turns into an antiresonance-resonance pair. This emission antiresonance-resonance pair is centered at $\hbar\omega = -|eV|/2$ and is fully identical to the absorption one.

As a result, the differential thermoelectric quantum noise becomes antisymmetric as a function of the frequency ω , that is the absorption and emission spectra are related as $\partial S^>(-\omega, V, V_T, \Delta\phi)/\partial V_T = -\partial S^>(\omega, V, V_T, \Delta\phi)/\partial V_T$. This is in contrast to the regime of low bias voltages where the absorption and emission spectra are in general not related to each other. Finally, we have analyzed the regime of large bias voltages and temperatures. It has been demonstrated that in this regime the antisymmetric relation between the absorption and emission spectra arises even when the QD is effectively coupled to a single MBS, that is at $\Delta\phi = 0$. However, when $\Delta\phi \neq 0$, the differential thermoelectric quantum noise acquires characteristic interference patterns in the absorption and emission spectra in such a way that the antisymmetric relation between these spectra does not break. This is in contrast to the system where the QD interacts with ABSs. In this system the differential thermoelectric quantum noise induced by ABSs is strongly suppressed in the low temperature regime both for small and large bias voltages whereas in the high temperature regime it does not exhibit any interference pattern for $\Delta\phi \neq 0$ and is only characterized by a simple shift to positive frequencies, that is to the absorption side, which obviously breaks the antisymmetric relation between the absorption and emission spectra.

The regime of large bias voltages and temperatures might be attractive for experiments. Let us estimate the

bias voltages $|eV|$ and temperatures $k_B T$ at which experiments could be performed and compared with the results shown in Figs. 8 and 10 for the systems with MBSs and ABSs, respectively. As specified above, the largest energy scale in the problem is $|\eta_1|$ which is thus the upper bound for the bias voltage, $|eV| < |\eta_1|$. Taking into account that the largest energy scale must not exceed the induced superconducting gap Δ , we have $|\eta_1| \lesssim \Delta$. In Figs. 8 and 10 we have $k_B T = 2.0 \times 10^{-2} |\eta_1|$ which means that $k_B T \lesssim 2.0 \times 10^{-2} \Delta$. Taking the value of Δ from a typical experiment, for example from Ref. [22], $\Delta \approx 250 \mu\text{eV}$, one obtains estimates for the bias voltage and thermal energy: $|eV| < 250 \mu\text{eV}$ and $k_B T \lesssim 5 \mu\text{eV}$. In terms of the temperature the latter estimate is equivalent to $T \lesssim 60 \text{mK}$. Therefore, the upper bounds for the bias voltages and temperatures corresponding to the results presented in Figs. 8 and 10 are about $250 \mu\text{eV}$ and 60mK , respectively. Since such bias voltages and temperatures are quite feasible, we hope that our results might be attractive for experimental measurements of the differential thermoelectric quantum noise of interfering MBSs at finite frequencies.

ACKNOWLEDGMENTS

The author thanks Reinhold Egger for a very useful discussion.

-
- [1] A. Yu. Kitaev, "Unpaired Majorana fermions in quantum wires," *Phys.-Usp.* **44**, 131 (2001).
 - [2] J. Alicea, "New directions in the pursuit of Majorana fermions in solid state systems," *Rep. Prog. Phys.* **75**, 076501 (2012).
 - [3] M. Leijnse and K. Flensberg, "Introduction to topological superconductivity and Majorana fermions," *Semicond. Sci. Technol.* **27**, 124003 (2012).
 - [4] M. Sato and S. Fujimoto, "Majorana fermions and topology in superconductors," *J. Phys. Soc. Japan* **85**, 072001 (2016).
 - [5] R. Aguado, "Majorana quasiparticles in condensed matter," *La Rivista del Nuovo Cimento* **40**, 523 (2017).
 - [6] R. M. Lutchyn, E. P. A. M. Bakkers, L. P. Kouwenhoven, P. Krogstrup, C. M. Marcus, and Y. Oreg, "Majorana zero modes in superconductor-semiconductor heterostructures," *Nat. Rev. Mater.* **3**, 52 (2018).
 - [7] A. Tsintzis, R. S. Souto, and M. Leijnse, "Creating and detecting poor man's Majorana bound states in interacting quantum dots," *Phys. Rev. B* **106**, L201404 (2022).
 - [8] P. Marra, "Majorana nanowires for topological quantum computation," *J. Appl. Phys.* **132**, 231101 (2022).
 - [9] T. Dvir, G. Wang, N. van Loo, C.-X. Liu, G. P. Mazur, A. Bordin, S. L. D. ten Haaf, J.-Y. Wang, D. van Driel, F. Zatelli, X. Li, F. K. Malinowski, S. Gazibegovic, G. Badawy, E. P. A. M. Bakkers, M. Wimmer, and L. P. Kouwenhoven, "Realization of a minimal Kitaev chain in coupled quantum dots," *Nature* **614**, 445 (2023).
 - [10] B. Muralidharan, M. Kumar, and C. Li, "Emerging quantum hybrid systems for non-Abelian-state manipulation," *Front. Nanotechnol.* **5**, 1219975 (2023).
 - [11] A. Tsintzis, R. S. Souto, K. Flensberg, J. Danon, and M. Leijnse, "Majorana qubits and non-Abelian physics in quantum dot-based minimal Kitaev chains," *PRX Quantum* **5**, 010323 (2024).
 - [12] Y. Tanaka, S. Tamura, and J. Cayao, "Theory of Majorana zero modes in unconventional superconductors," *Prog. Theor. Exp. Phys.*, ptae065 (2024).
 - [13] A. Yu. Kitaev, "Fault-tolerant quantum computation by anyons," *Ann. Phys.* **303**, 2 (2003).
 - [14] E. Majorana, "Teoria simmetrica dell'elettrone e del positrone," *Nuovo Cimento* **14**, 171 (1937).
 - [15] C. Itzykson and J.-B. Zuber, *Quantum Field Theory* (McGraw-Hill, New York, St. Louis, San Francisco, 1980).
 - [16] S. Smirnov, "Majorana tunneling entropy," *Phys. Rev. B* **92**, 195312 (2015).
 - [17] E. Sela, Y. Oreg, S. Plugge, N. Hartman, S. Lüscher, and J. Folk, "Detecting the universal fractional entropy of Majorana zero modes," *Phys. Rev. Lett.* **123**, 147702 (2019).
 - [18] S. Smirnov, "Majorana entropy revival via tunneling phases," *Phys. Rev. B* **103**, 075440 (2021).
 - [19] S. Smirnov, "Majorana ensembles with fractional entropy and conductance in nanoscopic systems," *Phys. Rev. B* **104**, 205406 (2021).

- [20] P. Yu, J. Chen, M. Gomanko, G. Badawy, E. P. A. M. Bakkers, K. Zuo, V. Mourik, and S. M. Frolov, “Non-Majorana states yield nearly quantized conductance in proximatized nanowires,” *Nat. Phys.* **17**, 482 (2021).
- [21] S. Frolov, “Quantum computing’s reproducibility crisis: Majorana fermions,” *Nature (London)* **592**, 350 (2021).
- [22] V. Mourik, K. Zuo, S. M. Frolov, S. R. Plissard, E. P. A. M. Bakkers, and L. P. Kouwenhoven, “Signatures of Majorana fermions in hybrid superconductor-semiconductor nanowire devices,” *Science* **336**, 1003 (2012).
- [23] S. Nadj-Perge, I. K. Drozdov, J. Li, H. Chen, S. Jeon, J. Seo, A. H. MacDonald, B. A. Bernevig, and A. Yazdani, “Observation of Majorana fermions in ferromagnetic atomic chains on a superconductor,” *Science* **346**, 602 (2014).
- [24] Z. Wang, H. Song, D. Pan, Z. Zhang, W. Miao, R. Li, Z. Cao, G. Zhang, L. Liu, L. Wen, R. Zhuo, D. E. Liu, K. He, R. Shang, J. Zhao, and H. Zhang, “Plateau regions for zero-bias peaks within 5% of the quantized conductance value $2e^2/h$,” *Phys. Rev. Lett.* **129**, 167702 (2022).
- [25] N. Hartman, C. Olsen, S. Lüscher, M. Samani, S. Fallahi, G. C. Gardner, M. Manfra, and J. Folk, “Direct entropy measurement in a mesoscopic quantum system,” *Nat. Phys.* **14**, 1083 (2018).
- [26] Y. Kleeorin, H. Thierschmann, H. Buhmann, A. Georges, L. W. Molenkamp, and Y. Meir, “How to measure the entropy of a mesoscopic system via thermoelectric transport,” *Nat. Commun.* **10**, 5801 (2019).
- [27] E. Pyurbeeva and J. A. Mol, “A thermodynamic approach to measuring entropy in a few-electron nanodevice,” *Entropy* **23**, 640 (2021).
- [28] T. Child, O. Sheekey, S. Lüscher, S. Fallahi, G. C. Gardner, M. Manfra, and J. Folk, “A robust protocol for entropy measurement in mesoscopic circuits,” *Entropy* **24**, 417 (2022).
- [29] C. Han, Z. Iftikhar, Y. Kleeorin, A. Anthore, F. Pierre, Y. Meir, A. K. Mitchell, and E. Sela, “Fractional entropy of multichannel Kondo systems from conductance-charge relations,” *Phys. Rev. Lett.* **128**, 146803 (2022).
- [30] E. Pyurbeeva, J. A. Mol, and P. Gehring, “Electronic measurements of entropy in meso- and nanoscale systems,” *Chem. Phys. Rev.* **3**, 041308 (2022).
- [31] T. Child, O. Sheekey, S. Lüscher, S. Fallahi, G. C. Gardner, M. Manfra, A. Mitchell, E. Sela, Y. Kleeorin, Y. Meir, and J. Folk, “Entropy measurement of a strongly coupled quantum dot,” *Phys. Rev. Lett.* **129**, 227702 (2022).
- [32] D. E. Liu and H. U. Baranger, “Detecting a Majorana-fermion zero mode using a quantum dot,” *Phys. Rev. B* **84**, 201308(R) (2011).
- [33] L. Fidkowski, J. Alicea, N. H. Lindner, R. M. Lutchyn, and M. P. A. Fisher, “Universal transport signatures of Majorana fermions in superconductor-Luttinger liquid junctions,” *Phys. Rev. B* **85**, 245121 (2012).
- [34] E. Prada, P. San-Jose, and R. Aguado, “Transport spectroscopy of NS nanowire junctions with Majorana fermions,” *Phys. Rev. B* **86**, 180503(R) (2012).
- [35] F. Pientka, G. Kells, A. Romito, P. W. Brouwer, and F. von Oppen, “Enhanced zero-bias Majorana peak in the differential tunneling conductance of disordered multisubband quantum-wire/superconductor junctions,” *Phys. Rev. Lett.* **109**, 227006 (2012).
- [36] C.-H. Lin, J. D. Sau, and S. Das Sarma, “Zero-bias conductance peak in Majorana wires made of semiconductor/superconductor hybrid structures,” *Phys. Rev. B* **86**, 224511 (2012).
- [37] M. Lee, J. S. Lim, and R. López, “Kondo effect in a quantum dot side-coupled to a topological superconductor,” *Phys. Rev. B* **87**, 241402(R) (2013).
- [38] A. Kundu and B. Seradjeh, “Transport signatures of Floquet Majorana fermions in driven topological superconductors,” *Phys. Rev. Lett.* **111**, 136402 (2013).
- [39] E. Vernek, P. H. Penteado, A. C. Seridonio, and J. C. Egues, “Subtle leakage of a Majorana mode into a quantum dot,” *Phys. Rev. B* **89**, 165314 (2014).
- [40] R. Ilan, J. H. Bardarson, H.-S. Sim, and J. E. Moore, “Detecting perfect transmission in Josephson junctions on the surface of three dimensional topological insulators,” *New J. Phys.* **16**, 053007 (2014).
- [41] A. M. Lobos and S. Das Sarma, “Tunneling transport in NSN Majorana junctions across the topological quantum phase transition,” *New J. Phys.* **17**, 065010 (2015).
- [42] Y. Peng, F. Pientka, Y. Vinkler-Aviv, L. I. Glazman, and F. von Oppen, “Robust Majorana conductance peaks for a superconducting lead,” *Phys. Rev. Lett.* **115**, 266804 (2015).
- [43] G. Sharma and S. Tewari, “Tunneling conductance for Majorana fermions in spin-orbit coupled semiconductor-superconductor heterostructures using superconducting leads,” *Phys. Rev. B* **93**, 195161 (2016).
- [44] B. van Heck, R. M. Lutchyn, and L. I. Glazman, “Conductance of a proximitized nanowire in the Coulomb blockade regime,” *Phys. Rev. B* **93**, 235431 (2016).
- [45] S. Das Sarma, A. Nag, and J. D. Sau, “How to infer non-Abelian statistics and topological visibility from tunneling conductance properties of realistic Majorana nanowires,” *Phys. Rev. B* **94**, 035143 (2016).
- [46] R. M. Lutchyn and L. I. Glazman, “Transport through a Majorana island in the strong tunneling regime,” *Phys. Rev. Lett.* **119**, 057002 (2017).
- [47] I. Weymann and K. P. Wójcik, “Transport properties of a hybrid Majorana wire-quantum dot system with ferromagnetic contacts,” *Phys. Rev. B* **95**, 155427 (2017).
- [48] V. L. Campo, Jr., L. S. Ricco, and A. C. Seridonio, “Isolating Majorana fermions with finite Kitaev nanowires and temperature: Universality of the zero-bias conductance,” *Phys. Rev. B* **96**, 045135 (2017).
- [49] C.-X. Liu, J. D. Sau, T. D. Stanescu, and S. Das Sarma, “Andreev bound states versus Majorana bound states in quantum dot-nanowire-superconductor hybrid structures: Trivial versus topological zero-bias conductance peaks,” *Phys. Rev. B* **96**, 075161 (2017).
- [50] H. Huang, Q.-F. Liang, D.-X. Yao, and Z. Wang, “Majorana ϕ_0 -junction in a disordered spin-orbit coupling nanowire with tilted magnetic field,” *Physica C: Superconductivity and its Applications* **543**, 22 (2017).
- [51] C.-X. Liu, J. D. Sau, and S. Das Sarma, “Distinguishing topological Majorana bound states from trivial Andreev bound states: Proposed tests through differential tunneling conductance spectroscopy,” *Phys. Rev. B* **97**, 214502 (2018).
- [52] Y.-H. Lai, J. D. Sau, and S. Das Sarma, “Presence versus absence of end-to-end nonlocal conductance correlations in Majorana nanowires: Majorana bound states versus Andreev bound states,” *Phys. Rev. B* **100**,

- 045302 (2019).
- [53] L.-W. Tang and W.-G. Mao, “Detection of Majorana bound states by sign change of the tunnel magnetoresistance in a quantum dot coupled to ferromagnetic electrodes,” *Front. Phys.* **8**, 147 (2020).
- [54] G. Zhang and C. Spånslätt, “Distinguishing between topological and quasi Majorana zero modes with a dissipative resonant level,” *Phys. Rev. B* **102**, 045111 (2020).
- [55] F. Chi, T.-Y. He, and G. Zhou, “Photon-assisted average current through a quantum dot coupled to Majorana bound states,” *J. Nanoelectron. Optoelectron.* **16**, 1325 (2021).
- [56] T. H. Galambos, F. Ronetti, B. Hetényi, D. Loss, and J. Klinovaja, “Crossed Andreev reflection in spin-polarized chiral edge states due to the Meissner effect,” *Phys. Rev. B* **106**, 075410 (2022).
- [57] J. Jin and X.-Q. Li, “Master equation approach for transport through Majorana zero modes,” *New J. Phys.* **24**, 093009 (2022).
- [58] W.-K. Zou, N.-W. Li, and F.-L. Chong, “Charge and spin transports through a normal lead coupled to an s-wave superconductor and Majorana fermions,” *Phys. Status Solidi B*, 2200472 (2023).
- [59] A. Hugué, K. Wrześniewski, and I. Weymann, “Spin effects on transport and zero-bias anomaly in a hybrid Majorana wire-quantum dot system,” *Sci. Rep.* **13**, 17279 (2023).
- [60] V. F. Becerra, M. Trif, and T. Hyart, “Quantized spin pumping in topological ferromagnetic-superconducting nanowires,” *Phys. Rev. Lett.* **130**, 237002 (2023).
- [61] A. Ziesen, A. Altland, R. Egger, and F. Hassler, “Statistical Majorana bound state spectroscopy,” *Phys. Rev. Lett.* **130**, 106001 (2023).
- [62] C.-Z. Yao, H.-L. Lai, and W.-M. Zhang, “Quantum transport theory of hybrid superconducting systems,” *Phys. Rev. B* **108**, 195402 (2023).
- [63] R. Taranko, K. Wrześniewski, I. Weymann, and T. Domański, “Transient effects in quantum dots contacted via topological superconductor,” *Phys. Rev. B* **110**, 035413 (2024).
- [64] M. Leijnse, “Thermoelectric signatures of a Majorana bound state coupled to a quantum dot,” *New J. Phys.* **16**, 015029 (2014).
- [65] R. López, M. Lee, L. Serra, and J. S. Lim, “Thermoelectrical detection of Majorana states,” *Phys. Rev. B* **89**, 205418 (2014).
- [66] H. Khim, R. López, J. S. Lim, and M. Lee, “Thermoelectric effect in the Kondo dot side-coupled to a Majorana mode,” *Eur. Phys. J. B* **88**, 151 (2015).
- [67] J. P. Ramos-Andrade, O. Ávalos-Ovando, P. A. Orellana, and S. E. Ulloa, “Thermoelectric transport through Majorana bound states and violation of Wiedemann-Franz law,” *Phys. Rev. B* **94**, 155436 (2016).
- [68] L. S. Ricco, F. A. Dessotti, I. A. Shelykh, M. S. Figueira, and A. C. Seridonio, “Tuning of heat and charge transport by Majorana fermions,” *Sci. Rep.* **8**, 2790 (2018).
- [69] S. Smirnov, “Dual Majorana universality in thermally induced nonequilibrium,” *Phys. Rev. B* **101**, 125417 (2020).
- [70] Z.-H. Wang and W.-C. Huang, “Dual negative differential of heat generation in a strongly correlated quantum dot side-coupled to Majorana bound states,” *Front. Phys.* **9**, 727934 (2021).
- [71] T.-Y. He, H. Sun, and G. Zhou, “Photon-assisted Seebeck effect in a quantum dot coupled to Majorana zero modes,” *Front. Phys.* **9**, 687438 (2021).
- [72] D. Giuliano, A. Nava, R. Egger, P. Sodano, and F. Buccheri, “Multiparticle scattering and breakdown of the Wiedemann-Franz law at a junction of N interacting quantum wires,” *Phys. Rev. B* **105**, 035419 (2022).
- [73] F. Buccheri, A. Nava, R. Egger, P. Sodano, and D. Giuliano, “Violation of the Wiedemann-Franz law in the topological Kondo model,” *Phys. Rev. B* **105**, L081403 (2022).
- [74] N. Bondyopadhyaya and D. Roy, “Nonequilibrium electrical, thermal and spin transport in open quantum systems of topological superconductors, semiconductors and metals,” *J. Stat. Phys.* **187**, 11 (2022).
- [75] W.-K. Zou, Q. Wang, and H.-K. Zhao, “Aharonov-Bohm oscillations in the Majorana fermion modulated charge and heat transports through a double-quantum-dot interferometer,” *Phys. Lett. A* **443**, 128219 (2022).
- [76] C. Wang and X.-Q. Wang, “Thermoelectric signature of Majorana zero modes in a T-typed double-quantum-dot structure,” *Chin. Phys. B* **32**, 037304 (2023).
- [77] W.-K. Zou, Q. Wang, and H.-K. Zhao, “Dynamic heat and charge transports through double-quantum-dot-interferometer modulated by Majorana bound states and time-oscillating Aharonov-Bohm flux,” *J. Phys. Condens. Matter* **35**, 165303 (2023).
- [78] F. Chi, J. Liu, Z. Fu, L. Liu, and Z. Yi, “Nonlinear Seebeck and Peltier effects in a Majorana nanowire coupled to leads,” *Chin. Phys. B* **33**, 077301 (2024).
- [79] S. Mishra, R. Das, and C. Benjamin, “Majorana thermoelectrics and refrigeration,” *J. Appl. Phys.* **136**, 234401 (2024).
- [80] P. Trocha, T. Jonckheere, J. Rech, and T. Martin, “Thermoelectric properties of a quantum dot attached to normal metal and topological superconductor,” *Sci. Rep.* **15**, 3068 (2025).
- [81] D. E. Liu, M. Cheng, and R. M. Lutchyn, “Probing Majorana physics in quantum-dot shot-noise experiments,” *Phys. Rev. B* **91**, 081405(R) (2015).
- [82] D. E. Liu, A. Levchenko, and R. M. Lutchyn, “Majorana zero modes choose Euler numbers as revealed by full counting statistics,” *Phys. Rev. B* **92**, 205422 (2015).
- [83] A. Haim, E. Berg, F. von Oppen, and Y. Oreg, “Current correlations in a Majorana beam splitter,” *Phys. Rev. B* **92**, 245112 (2015).
- [84] S. Valentini, M. Governale, R. Fazio, and F. Taddei, “Finite-frequency noise in a topological superconducting wire,” *Physica E* **75**, 15 (2016).
- [85] A. Zazunov, R. Egger, and A. Levy Yeyati, “Low-energy theory of transport in Majorana wire junctions,” *Phys. Rev. B* **94**, 014502 (2016).
- [86] S. Smirnov, “Non-equilibrium Majorana fluctuations,” *New J. Phys.* **19**, 063020 (2017).
- [87] T. Jonckheere, J. Rech, A. Zazunov, R. Egger, A. Levy Yeyati, and T. Martin, “Giant shot noise from Majorana zero modes in topological trijunctions,” *Phys. Rev. Lett.* **122**, 097003 (2019).
- [88] D. Bathellier, L. Raymond, T. Jonckheere, J. Rech, A. Zazunov, and T. Martin, “Finite frequency noise in a normal metal - topological superconductor junction,” *Phys. Rev. B* **99**, 104502 (2019).

- [89] S. Smirnov, “Majorana finite-frequency nonequilibrium quantum noise,” *Phys. Rev. B* **99**, 165427 (2019).
- [90] J. Manousakis, C. Wille, A. Altland, R. Egger, K. Flensberg, and F. Hassler, “Weak measurement protocols for Majorana bound state identification,” *Phys. Rev. Lett.* **124**, 096801 (2020).
- [91] S. Smirnov, “Revealing universal Majorana fractionalization using differential shot noise and conductance in nonequilibrium states controlled by tunneling phases,” *Phys. Rev. B* **105**, 205430 (2022).
- [92] G.-H. Feng and H.-H. Zhang, “Probing robust Majorana signatures by crossed Andreev reflection with a quantum dot,” *Phys. Rev. B* **105**, 035148 (2022).
- [93] Z. Cao, G. Zhang, H. Zhang, Y.-X. Liang, W.-X. He, K. He, and D. E. Liu, “Differential current noise as an identifier of Andreev bound states that induce nearly quantized conductance plateaus,” *Phys. Rev. B* **108**, L121407 (2023).
- [94] S. Smirnov, “Nonequilibrium finite frequency resonances in differential quantum noise driven by Majorana interference,” *Phys. Rev. B* **109**, 195410 (2024).
- [95] S. Smirnov, “Universal Majorana thermoelectric noise,” *Phys. Rev. B* **97**, 165434 (2018).
- [96] S. Smirnov, “Dynamic Majorana resonances and universal symmetry of nonequilibrium thermoelectric quantum noise,” *Phys. Rev. B* **100**, 245410 (2019).
- [97] S. Smirnov, “Majorana differential shot noise and its universal thermoelectric crossover,” *Phys. Rev. B* **107**, 155416 (2023).
- [98] J.-F. Ge, K. M. Bastiaans, D. Chatzopoulos, D. Cho, W. O. Tromp, T. Benschop, J. Niu, G. Gu, and M. P. Allan, “Single-electron charge transfer into putative Majorana and trivial modes in individual vortices,” *Nat. Commun.* **14**, 3341 (2023).
- [99] J. Basset, A. Y. Kasumov, C. P. Moca, G. Zaránd, P. Simon, H. Bouchiat, and R. Deblock, “Measurement of quantum noise in a carbon nanotube quantum dot in the Kondo regime,” *Phys. Rev. Lett.* **108**, 046802 (2012).
- [100] M. Gau, R. Egger, A. Zazunov, and Y. Gefen, “Towards dark space stabilization and manipulation in driven dissipative Majorana platforms,” *Phys. Rev. B* **102**, 134501 (2020).
- [101] M. Gau, R. Egger, A. Zazunov, and Yuval Gefen, “Driven dissipative Majorana dark spaces,” *Phys. Rev. Lett.* **125**, 147701 (2020).
- [102] M.-T. Deng, S. Vaitiekėnas, E. Prada, P. San-Jose, J. Nygård, P. Krogstrup, R. Aguado, and C. M. Marcus, “Nonlocality of Majorana modes in hybrid nanowires,” *Phys. Rev. B* **98**, 085125 (2018).
- [103] D. A. Ruiz-Tijerina, E. Vernek, L. G. G. V. Dias da Silva, and J. C. Egues, “Interaction effects on a Majorana zero mode leaking into a quantum dot,” *Phys. Rev. B* **91**, 115435 (2015).
- [104] K. Flensberg, “Non-Abelian operations on Majorana fermions via single-charge control,” *Phys. Rev. Lett.* **106**, 090503 (2011).
- [105] J. Fuchs and C. Schweigert, *Symmetries, Lie Algebras and Representations, a Graduate Course for Physicists* (Cambridge University Press, Cambridge, 1997).
- [106] A. Altland and B. Simons, *Condensed Matter Field Theory*, 2nd ed. (Cambridge University Press, Cambridge, 2010).
- [107] L. V. Keldysh, “Diagram technique for nonequilibrium processes,” *Sov. Phys. JETP* **20**, 1018 (1965).
- [108] A. C. Hewson, *The Kondo Problem to Heavy Fermions* (Cambridge University Press, Cambridge, 1997).
- [109] S. Smirnov and M. Grifoni, “Slave-boson Keldysh field theory for the Kondo effect in quantum dots,” *Phys. Rev. B* **84**, 125303 (2011).
- [110] M. Niklas, S. Smirnov, D. Mantelli, M. Margańska, N.-V. Nguyen, W. Wernsdorfer, J.-P. Cleuziou, and M. Grifoni, “Blocking transport resonances via Kondo many-body entanglement in quantum dots,” *Nat. Commun.* **7**, 12442 (2016).
- [111] M. Cheng, M. Becker, B. Bauer, and R. M. Lutchyn, “Interplay between Kondo and Majorana interactions in quantum dots,” *Phys. Rev. X* **4**, 031051 (2014).
- [112] I. Weymann, K. P. Wójcik, and P. Majek, “Majorana-Kondo interplay in T-shaped double quantum dots,” *Phys. Rev. B* **101**, 235404 (2020).
- [113] P. Majek, K. P. Wójcik, and I. Weymann, “Spin-resolved thermal signatures of Majorana-Kondo interplay in double quantum dots,” *Phys. Rev. B* **105**, 075418 (2022).
- [114] K. P. Wójcik, T. Domański, and I. Weymann, “Signatures of Kondo-Majorana interplay in ac response,” *Phys. Rev. B* **109**, 075432 (2024).